hnRNPs Interacting with mRNA Localization Motifs Define Axonal RNA Regulons*[S]

Seung Joon Lee‡, Juan A. Oses-Prieto§, Riki Kawaguchi¶, Pabitra K. Sahoo‡, Amar N. Kar‡, Meir Rozenbaum‖, David Oliver**, Shreya Chand§, Hao Ji**, Michael Shtutman**, Sharmina Miller-Randolph‡, Ross J. Taylor‡, Mike Fainzilber‖, Giovanni Coppola¶‡‡, Alma L. Burlingame§, and Jeffery L. Twiss‡§§

mRNA translation in axons enables neurons to introduce new proteins at sites distant from their cell body. mRNA-protein interactions drive this post-transcriptional regulation, yet knowledge of RNA binding proteins (RBP) in axons is limited. Here we used proteomics to identify RBPs interacting with the axonal localizing motifs of *Nrn1*, *Hmgb1*, *Actb*, and *Gap43* mRNAs, revealing many novel RBPs in axons. Interestingly, no RBP is shared between all four RNA motifs, suggesting graded and overlapping specificities of RBP-mRNA pairings. A systematic assessment of axonal mRNAs interacting with hnRNP H1, hnRNP F, and hnRNP K, proteins that bound with high specificity to *Nrn1* and *Hmgb1*, revealed that axonal mRNAs segregate into axon growth-associated RNA regulons based on hnRNP interactions. Axotomy increases axonal transport of hnRNPs H1, F, and K, depletion of these hnRNPs decreases axon growth and reduces axonal mRNA levels and axonal protein synthesis. Thus, subcellular hnRNP-interacting RNA regulons support neuronal growth and regeneration. *Molecular & Cellular Proteomics 17: 2091–2106, 2018. DOI: 10.1074/mcp.RA118.000603.*

mRNAs are actively transported into axons where they are used to synthesize new proteins (1). These locally generated proteins contribute to growth and function of axons as well as retrograde signaling for injury responses and survival in the peripheral nervous system (PNS)[1] (2, 3). The transport of mRNAs into axons and their translation within axons can be regulated by extracellular stimuli (4). RNA binding proteins (RBPs) interacting with structural motifs within these mRNAs drive these post-transcriptional mechanisms (5). For example, zip-code binding protein 1 (ZBP1, also called IGF-II mRNA binding (IMP1)) protein was shown to bind to a 56 nucleotide (nt) stem-loop structure in the 3′ untranslated region (UTR) of *β-actin* mRNA (*Actb*), and this binding is necessary for axonal transport of the mRNA (6, 7). Other RBPs implicated in axonal mRNA transport include nucleolin (Ncl), HuD (also called ELAVL4), hnRNP Q, hnRNP R, splicing factor proline and glutamine-rich (SFPQ), fragile X mental retardation (FMRP), Hermes, TRF2-S, and TDP-43 proteins (8–17). Despite increased insight into RNA transport and translation, including the identification of literally thousands of axonal mRNAs (18, 19), relatively few RBPs have been identified in axons.

In other cellular systems, mRNAs encoding proteins with complementary functions have been shown to share RBPs that regulate their stability (20). This led to the notion of "RNA regulons," where cohorts of mRNAs encoding proteins with complementary functions are co-regulated by shared RBPs. However, it is not known if the RNA regulon concept applies to subcellular compartments. Here, we have used axonal RNA localization motifs as "bait" coupled with mass spectrometry (MS) to identify the RBPs that bind to *Nrn1* (also called *Cortical Plasticity Gene 15*), *Hmgb1* (also called *Amphoterin*), *Actb,* and *Gap43* mRNA localization motifs. Many interacting proteins were uncovered for each motif by this RNA affinity MS (RAMS) approach, but we found no protein shared by all four motifs. This suggests that pairing combinations of RBPs with localization motifs provides a level of specificity for axonal mRNA cohorts. RNA co-immunoprecipitation (RIP) with axonal heterogeneous nuclear ribonucleoproteins (hnRNPs) H1, F, and K, which showed high specificity binding to the *Nrn1* and *Hmgb1* mRNA motifs, segregates the axonal mRNA populations into binding cohorts, thus defining axon growth-associated RNA regulons based on hnRNP interactions. Consistent with this link to axon growth, axotomy increases axonal transport of hnRNP H1, F, and K, and depletion of these hnRNPs decreases axon growth and axonal protein synthesis.

From the ‡Department of Biological Sciences, University of South Carolina, Columbia, SC, 29208; §Department of Pharmaceutical Chemistry, University of California San Francisco, San Francisco, CA, 94158; ¶Department of Psychiatry and Semel Institute for Neuroscience and Human Behavior, David Geffen School of Medicine, University of California Los Angeles, Los Angeles, CA 90095; ‖Department of Biomolecular Sciences, Weizmann Institute of Science, Rehovot, 76100, Israel; **Department of Drug Discovery and Biomedical Sciences, University of South Carolina, Columbia, SC, 29208; ‡‡Department of Neurology, David Geffen School of Medicine, University of California Los Angeles, Los Angeles, CA, 90095

Received January 14, 2018, and in revised form, July 5, 2018
Published, MCP Papers in Press, July 23, 2018, DOI 10.1074/mcp.RA118.000603

EXPERIMENTAL PROCEDURES

Animal Use and Neuron Cultures—All animal experiments were approved by institutional IACUC. 150–175 g adult male Sprague-Dawley rats were used for all experiments. Sciatic nerve crush injury and DRG cultures were performed as described (21). Dissociated L4–6 DRGs were cultured on poly-L-lysine (Sigma, St. Louis, MO) plus laminin (Millipore) coated coverslips or polyethylene-tetrathalate (PET) membrane inserts (1 μm pores; Falcon, Corning, NY). Axons were isolated from DRGs cultured on PET membranes as described (22).

For transfection, dissociated ganglia were pelleted at 100 $\times$ *g* for 5 min and resuspended in 20 μl nucleofector solution (Basic Neuron SCN Nucleofector kit; Lonza, Walkersville, MD). 2–3 μg of plasmid was electroporated using the Amaxa Nucleofector™ II device (program SCN-8; Lonza).

For siRNA transfections, 100 nM siRNA pools (Dharmacon, Lafayette, CO) were transfected using DharmaFECT 3 reagent (Dharmacon) at 3 h after plating DRGs. The siRNA sequences used in this study are shown in supplemental Table S1. Non-targeting siRNAs (siCon; Dharmacon) were used as control. In some experiments, DRGs were transfected a second time with 100 nM siRNAs at 4 d *in vitro* (DIV), and then replated on DIV 6 as described (23).

Isolation of Sciatic Nerve Axoplasm—Axoplasm was obtained from rat sciatic nerve by extrusion in nuclear transport buffer (20 mM HEPES (pH 7.3), 110 mM potassium acetate, 5 mM magnesium acetate) supplemented with protease/phosphatase inhibitor mixture (Roche, Basel, Switzerland) and RNasin Plus (Promega, Madison, WI) as described (24). Axoplasm preparations were cleared by centrifugation at 20,000 $\times$ *g*, 4 °C for 15 min and then processed for RNA affinity binding, immunoblotting, or immunoprecipitations as below. For crushed nerves, axoplasm was harvested proximal to the injury site. For naïve nerves, axoplasm was harvested from equal length of nerve taken from approximately the same anatomic location as the crushed nerves.

DNA Constructs—Myristoylated EGFP (GFP^{MYR}) was used to screen for axonal localization by UTRs. GFP^{MYR}-5′nrn1/3′γ-actin construct has been previously described (25). The 1–94 and 95–188 nt segments of Nrn1 were generated by PCR and inserted restriction enzyme sites (AflII/BamHI) were used to replace the full length 5′UTR in GFP^{MYR}-5′nrn1/3′γ-actin construct. Bidirectional sequencing validated all amplified cDNA inserts.

Fluorescence In Situ Hybridization (FISH) and Immunofluorescence—For FISH/IF, transfected DRG neurons were fixed for 15 min in 4% paraformaldehyde (PFA). Digoxigenin (DIG) labeled GFP antisense cRNA probes were used to detect GFP as described; DIG labeled sense probes were used for control (26). Immunofluorescence for neurofilament (NF) was used to visualize neurons.

Immunofluorescence was performed as described (26). 4% PFA was used for fixation of all antibodies, except for anti-hnRNP K where ice-cold methanol was used. Primary antibodies consisted of rabbit anti-hnRNP H1 (Abcam, Cambridge, MA, 1:200), mouse anti-hnRNP K (Abcam, 1:200), rabbit anti-PurA (Abcam, 1:200) and a mixture of chicken anti-NF H, -NF M and -NF L (Aves labs, Tigard, OR, 1:500). FITC-conjugated donkey anti-rabbit, anti-mouse and Cy5-conjugated donkey anti-mouse (Jackson ImmunoResearch, West Grove, PA, 1:200) were used as secondary antibodies.

Coverslips were mounted with Prolong Gold (Invitrogen, Waltham, MA). Fluorescent signals were captured with Leica DMI6000 epifluorescence microscope (Buffalo Grove, IL) and ORCA Flash ER CCD camera (Hamamatsu, Shizuoka Prefecture, Japan) using matched acquisition parameters (exposure time and gain) and any post-processing.

RNA Affinity Chromatography—RNA-protein pull-down for the RAMS procedure was performed as described (27). Briefly, biotin-conjugated RNA oligonucleotides (TriLink, San Diego, CA) were coupled to *Streptavidin Dynabeads* (SA; Invitrogen). After clearing, axoplasm from 7 d injury-conditioned rat sciatic nerve was incubated with oligonucleotide-bound beads for 4 h at 4 °C. Beads were precipitated using a magnetic rack and then washed extensively with 10 mM HEPES (pH 7.4), 3 mM magnesium chloride, 250 mM sodium chloride, 1 mM DTT and 5% glycerol. Bound proteins were eluted with 50 μg/ml RNase A (Sigma). Denatured proteins were fractionated by SDS/PAGE and then stained with *Sypro Ruby* solution; gel lanes were excised for MS.

In-gel Digestion and Mass Spectrometry—Protein bands were digested in-gel with trypsin as described (28). The extracted digests were separated in a NanoAcquity™ Ultraperformance UPLC system (Waters, Milford, MA) with incorporated nanoemiter (Thermo Scientific, Waltham, MA). Mobile phase A was 0.1% formic acid in water and mobile phase B was 0.1% formic acid in acetonitrile. After equilibration of the column in 2% solvent B, an aliquot of each digest (5 μl) was injected, then the organic content of the mobile phase was increased linearly to 27% over 27 min, and then to 50% in 2 min. The liquid chromatography eluate was coupled to a hybrid linear ion trap-Orbitrap mass spectrometer (LTQ-Orbitrap Velos, Thermo Scientific). Peptides were analyzed in positive ion mode and in information-dependent acquisition mode to automatically switch between MS and MS/MS acquisition. MS spectra were acquired in profile mode using the Orbitrap analyzer in the m/z range between 350 and 1400.

Peaklists were generated using PAVA in-house software (29), based on the RawExtract Script from Xcalibur v2.4 (Thermo Scientific). The peak lists were searched against the rat + human subset of the UniProt database as of June 17, 2013 (167,793 entries), using in-house ProteinProspector version 5.10.10 (http://prospector.ucsf.edu/prospector/mshome.htm). A randomized version of all en-

[1] The abbreviations used are: PNS, peripheral nervous system; *Actb,* β-actin mRNA; Adv, Advillin; ddPCR, droplet digital PCR; DHH, desert hedgehog; DIG, digoxigenin; DIV, days in vitro; DRG, dorsal root ganglion; eIF2α, eukaryotic initiation factor 2α; ELAVL1, embryonic lethal, abnormal vision, drosophila-like protein 1; ELAVL4, embryonic lethal, abnormal vision, drosophila-like protein 4; FC, fold change; FDR, false discovery rate; FISH, fluorescent in situ hybridization; FLAG, flag octapeptide (DYKDDDDK) epitope tag; FMRP, fragile X mental retardation protein; *Gap43,* growth-associated protein 43 kDa; *Gapdh,* glutaraldehyde phosphate dehydrogenase mRNA; GAPDH, glutaraldehyde phosphate dehydrogenase protein; GFP, green fluorescent protein; GFP^{MYR}, green fluorescent protein with myristoylation motif; GO, gene ontology; Hmgb1, high mobility group binding protein 1; *Hmgb1,* high mobility group binding protein 1 mRNA; hnRNP, heterologous nuclear ribonucleoprotein; HuD, Hu-antigen D; HuR, Hu antigen R; IMP, IGFII mRNA binding protein 1; IP, immunoprecipitation; IPA, Ingenuity pathway analysis; La/SSB, Lupus antigen/single-stranded binding protein; Log2FC, log 2 fold change; Ncl, nucleolin protein; NF, neurofilament; *Nfm,* neurofilament medium mRNA; *Nrn1,* neuritin 1 mRNA; Nrn1, neuritin 1 protein; nt, nucleotide(s); PET, polyethylene-tetrathalate; PFA, paraformaldehyde; QC, quality control; RAMS, RNA affinity mass spectrometry; RBP, RNA binding protein; RIP, RNA co-immunoprecipitation; RRHO, rank-rank hypergeometric overlap; RT-ddPCR, reverse transcription-coupled droplet digital PCR; Runx3, runt related transcription factor 3; SA, streptavidin; SD, standard deviation; SEM, standard error of the mean; Seq, next-generation sequencing; SFPQ, splicing factor proline and glutamine rich; siCon, control siRNA (non-targeting); siRNA, small interfering RNA; UTR, untranslated region; ZBP1, zipcode binding protein 1.

tries was concatenated to the database for estimation of false discovery rates in the searches. Protein hits were considered significant when at least two peptide sequences matched a protein entry and the Prospector score was above the significance level. For identifications based on one single peptide sequence with high scores, the MS/MS spectrum was reinterpreted manually by matching all the observed fragment ions to a theoretical fragmentation obtained using MS Product (Protein Prospector) (30). supplemental Table S7 details protein identifications from single peptides with links for annotated spectra.

QSpec was used to determine the fold change (FC) between spectral counts of peptides bound to control or target RNA and the false discovery rates (FDR) (31). Log2FC cut offs were 0.7 and −0.7 and FDR cut off was 0.05. Normalized enrichment index compared with spectral counts normalized for protein molecular weight was used to incorporate binding to biotin control. Equation for calculating enrichment index is shown in in supplemental Table S2A.

RNA Immunoprecipitation (RIP)-Sequencing—Preclearing, primary antibody incubations, and precipitations were performed at 4 °C with rotation. Axoplasm isolates were precleared with *Protein A-Dynabeads* (Invitrogen) for 30 min, followed by incubation with primary antibodies for 3 h and then 2 h with *Protein G-Dynabeads* (Invitrogen). 5 μg each of the following primary antibodies were used: mouse anti-FLAG (Sigma), rabbit anti-hnRNP H1 (Abcam), mouse anti-hnRNP F (Thermo Scientific), mouse anti-hnRNP K (Abcam) and mouse anti-La/SSB (BD Biosciences, San Jose, CA) antibodies. Bound RNA was purified as above. For analyses by reverse transcription-coupled droplet digital PCR (RT-ddPCR), *SsoAdvanced PreAmp kit* (Bio-Rad, Hercules, CA) was used to pre-amplify cDNA for ddPCR per the manufacturer's protocol.

RNA-sequencing libraries were prepared using the NuGEN Ovation RNA Ultra Low Input kit (500 pg, San Carlos, CA) and TruSeq Nano (Illumina, San Diego, CA). Libraries were indexed and sequenced over 3 lanes by HiSeq4000 (Illumina) with 69 bp paired-end reads. Quality control (QC) was performed on base qualities and nucleotide composition of sequences, to identify problems in library preparation or sequencing. Reads were trimmed and filtered after the QC before input to the alignment stage. Reads were aligned to the latest rat Rn6 reference genome using the STAR spliced read aligner (ver 2.4.0). Average input read counts were 61.7 M and average percentage of uniquely aligned reads was 58%. Total counts of read-fragments aligned to known gene regions within the rat (rn6) Ensembl reference annotation were used as the basis for quantification of gene expression. Fragment counts were derived using HTSeq program (ver 0.6.0). RNAs with at least 10 counts in at least one condition across all replicates were retained for differential expression analysis, which was performed using EdgeR (ver 3.14.0).

Relative mRNA enrichment in the RNA-seq data sets for each RBP compared with both input and anti-FLAG RIP RNA using the online RRHO server (http://systems.crump.ucla.edu/rankrank/index.php) with step size set at 100 (32). Scripts used in the RNA sequencing analyses are available at https://github.com/icnn/RNAseq-PIPELINE.git. Raw and processed data were deposited within the Gene Expression Omnibus (GEO) repository (www.ncbi.nlm.nih.gov/geo, accession number: GSE103444).

Filtering RIP-seq Data Using Sensory Neuron-specific Translatomes—Sensory neuron specific translatome data were taken from a recent study that used RiboTag mice crossed with different Cre lines (Adv, Islt, Runx3, and Dhh) for cell specific expression (33). These translatome data were used to filter the axoplasm interactome lists for each RBP. For this, the Ribotag (mouse) and RIP-seq (rat) data were mapped to generate Ensembl gene names for each mRNA. dbOrtho (https://biodbnet-abcc.ncifcrf.gov/dbInfo/examples.php#dbOrtho) was then used to determine identities of overlapping mRNAs between the mouse and rat data sets. Rat orthologs were identified for more than 80% of the mouse genes from the neuron-specific translatome data set.

Motif Discovery in RBPs Interactome—Binding motifs enriched in the RBP-interacting mRNAs were analyzed by Homer motif discovery software (findMotifs.pl) (ver 4.9) (http://homer.ucsd.edu/homer/motif/index.html). We used the mouse refSeq with reported full-length mRNAs (5′UTR, CDS and 3′UTR) as source for motif discovery.

GO and IPA Analysis—Proteins identified by RAMS as interacting with different RNA oligonucleotides were examined for enrichment of GO terms using GOrilla (http://cbl-gorilla.cs.technion.ac.il/) (34). Target protein list and background list, which included all the proteins identified by MS, were submitted to identify enriched categories. The pathway enrichment analysis of the gene clusters was conducted with the R package *clusterProfiler* (35). The *Bioconductor* annotation packages GO.db, KEGG.db, and org.Hs.eg.db were used as references for the enrichment analysis.

Axonal mRNAs from RIP-Seq were examined for functional annotation by GO and IPA analysis. GO enrichment analysis was performed by submitting the list of mRNAs interacting with a hnRNP along with the background list to GOrilla. RBP-interacting mRNAs were mapped to canonical signaling pathways in the Ingenuity Pathways Knowledge Base using the entire list of mRNAs obtained by sequencing axoplasmic RNA as a background. One tailed Fisher's exact test was used to calculate the *p* value for nonrandom association of mRNA ensembles with a given pathway.

Subcellular Protein Fractionation—Dissociated DRG neurons were plated on porous membranes (3 μm pore diameter) and cultured for 3 d. After rinsing with PBS three times, lower membrane surfaces were scraped to collect the axonal fraction that was then lysed in 1× Laemmli buffer. The upper membrane surface was then harvested in 20 mM HEPES (pH 7.4), 10 mM KCl, 1 mM $MgCl_2$, 20% glycerol, 0.2% Triton X-100 and 1× protease inhibitor mixture (extraction buffer). Cells were lysed by gentle pipetting and then centrifuged at 15,000 × *g* for 20 min to pellet nuclei. Supernatant (cytoplasmic fraction) was denatured by addition of 4× Laemmli buffer. The pellet was washed three times with extraction buffer and then lysed with 1× Laemmli buffer as the nuclear fraction.

Immunoblotting—Protein lysates were quantified for yield by Bradford assay or BCA assay. Denatured protein lysates or aliquots from RIPs were fractionated by SDS-PAGE and transferred to PVDF or nitrocellulose membranes. For lysates, equivalent protein mass was used; for RIP analyses, protein yields were normalized prior to RIP, and then equivalent fractions of the RIPs were analyzed. After transfer, membranes were blocked and probed with primary and HRP-conjugated secondary antibodies as described (36). The following primary antibodies were used: rabbit anti-hnRNP H1 (Abcam, 1:5000), mouse anti-hnRNP F (Thermo Scientific, 1:1000), mouse anti-hnRNP H1/F (Abcam, 1:1000), mouse anti-hnRNP K (Abcam, 1:2000), rabbit anti-Elavl1/HuR (Cell Signaling, Danvers, MA, 1:1000), rabbit anti-Nucleolin (Abcam, 1:1000), rabbit anti-hnRNP A3 (LSBio, 1:1000), mouse anti-PurA (Abcam, 1:1000), rabbit anti-PurB (Novus, Littleton, CO, 1:1000), mouse anti-eIF2α (Cell Signaling, 1:1000), mouse anti-GAPDH (Abcam, 1:2000), mouse anti-Lamin A/C (Santa Cruz Biotechnology, San Diego, CA, 1:3000), and rabbit anti-αTubulin (Cell Signaling, 1:5000). HRP-conjugated anti-mouse or -rabbit antibodies (Cell Signaling, 1:2000) were used for secondaries. For detection of immunoprecipitated hnRNP proteins, anti-mouse and anti-rabbit Trueblot kit (Rockland, Pottstown, PA) was used to minimize detection of denatured IgGs. Immune complexes were detected with *ECL Prime*™ (GE Healthcare, Pittsburgh, PA).

RNA Isolation and PCR Analyses—RNA was isolated from dissociated DRG cultures using the *RNeasy Microisolation* kit and from whole DRGs using *Trizol* (Invitrogen). Fluorimetry with *Ribogreen* (Invitrogen) was used for RNA quantification. RNA samples were reverse

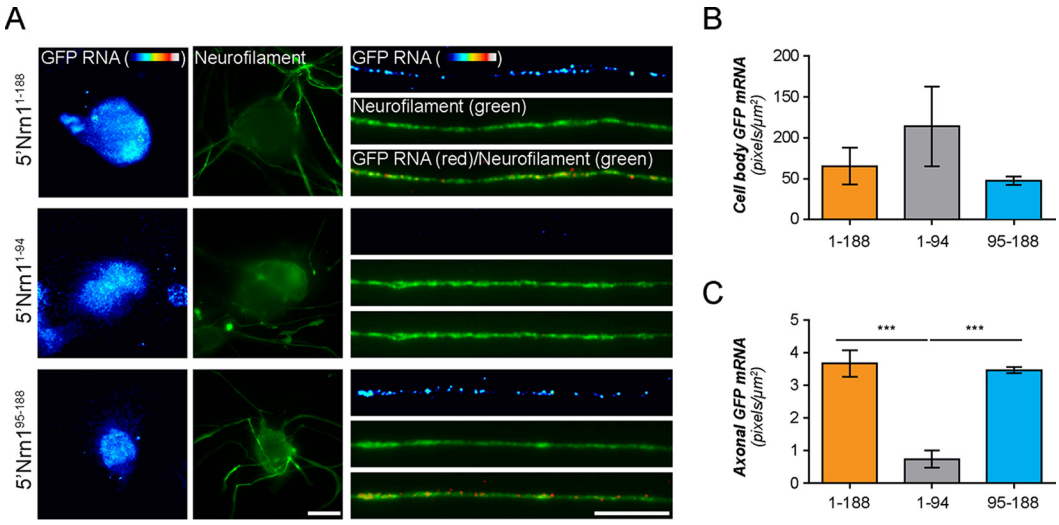

FIG. 1. **nt 95–188 in Nrn1's 5′UTR are sufficient for its axonal localization.** *A,* Representative fluorescent *in situ* hybridization images for *GFP* mRNA and immunofluorescent images for neurofilament (NF) protein in cell bodies and corresponding distal axons of cultured DRG neurons that were transfected with GFP^{MYR} plus nt 1–188, 1–94 or 95–188 of rat *Nrn1* (5′$Nrn1^{1-188}$, 5′$Nrn1^{1-94}$, and 5′$Nrn1^{95-188}$, respectively) are shown (Scale bars = 20 μm). *B-C,* Quantification of RNA signals in the cell body (*B*) and distal axons (*C*) from replicate cultures as in *A* are shown as mean pixel intensity ± S.E. (N ≥ 45 neurons over 3 separate culture/transfections; ***, $p < 0.001$ by one-way ANOVA with pair-wise comparison and Tukey post-hoc).

transcribed and used for ddPCR with either *Evagreen* (Bio-Rad) or *Taqman* (Integrated DNA Tech, Skokie, IL) detection.

Axon Growth Analyses—Images of neurons immunostained with anti-NF were acquired by tile-scanning of entire coverslips and analyzed by *WIS-Neuromath* (37) or *ImageJ* with *NeuronJ* plugin programs (National Institutes of Health).

Nascent Protein Synthesis Assay—To visualize newly synthesized proteins in cultured DRG neurons, *Click-iT™ Plus OPP Protein Synthesis Assay Kit* (Invitrogen) was used per manufacturer's instruction. Briefly, neurons were incubated with 20 μM O-propargyl-puromycin (OPP) for 30 min at 37 °C. OPP-labeled proteins were detected by crosslinking with Alexa Fluor-594 picolyl azide. Cells were fixed, and coverslips were mounted with *Prolong Gold Antifade* mounting solution (Invitrogen) and imaged with Leica DMI6000 epifluorescent microscope as above. Morphology from DIC imaging was used to visualize neuronal processes and cell bodies, and to distinguish neurons from glial cells. ImageJ was used to quantify the Puromycin signals in cell bodies and distal axons.

Experimental Design and Statistical Rationale—All experiments were performed in at least three biological replicates and are reported as mean ± standard deviation (S.D.) or standard error of the mean (S.E.) as indicated. Student's *t* test or one-way ANOVA with pairwise comparisons and Tukey post-hoc was used to determine significance differences between groups. *Prism* software (GraphPad, San Diego, CA) was used for all statistical analyses.

RESULTS

Defining the Axonal Localization Motif of Nrn1 mRNA—We had previously shown that intra-axonal translation of *Hmgb1* and *Nrn1* supports axon growth (25, 36). Axonal localization of *Hmgb1* mRNA is driven through a 60 nt motif in its 3′UTR, and the *Hmgb1* mRNA is constitutively transported into sensory axons (36). *Nrn1* mRNA's transport into axons is increased during regeneration and its 5′UTR drives its localization (25). We reasoned that the differential transport of these two mRNAs could be leveraged to test for possible occurrence of axonal RNA regulons, hence we sought to narrow down the 188 nt *Nrn1* mRNA 5′UTR to a shorter RNA segment suitable for RAMS (27). For this, we transfected rat primary dorsal root ganglion (DRG) neurons with a reporter mRNA containing varying portions of *Nrn1* mRNA 5′UTR (NCBI accession # NM_053346.1), the coding sequence of myristoylated GFP (GFP^{MYR}), and the non-localizing 3′UTR of *γ-actin* mRNA (*Actg*). As previously shown (25), *GFP* mRNA localized into axons when it included *Nrn1* mRNA nt 1–188. In contrast, GFP^{MYR} with *Nrn1* mRNA nt 1–94 showed axonal *GFP* mRNA signals indistinguishable from the sense probe (data not shown), whereas nt 95–188 revealed robust axonal *GFP* mRNA signals (Fig. 1*A*, 1*C*). Axonal localization of *GFP* mRNA was lost upon further deletions of nt 95–188 segment (data not shown), indicating that this 5′UTR region is necessary and sufficient for its axonal localization. *Nrn1* mRNA nt 95–188 shows higher sequence conservation across species than *Nrn1* mRNA nt 1–94 (supplemental Fig. S1*A*). Although an RBP can show primary sequence specificity, in many cases RBPs recognize motifs in the context of secondary structures (38). Secondary structure predictions using aligned *Nrn1* sequences show a stem-loop RNA structure for nt 95–188 compared with relatively unstructured nt 1–94 (supplemental Fig. S1*B*–S1*C*). These findings indicate that *Nrn1* mRNA's nt 95–188 may serve as a binding motif for axonal RBPs.

Distinct Axonal Protein Populations Bind to the Localizing Motifs of Nrn1, Hmgb1, Actb, and Gap43 mRNAs—We used RAMS with biotinylated RNA oligonucleotides to identify RBPs in sciatic nerve axoplasm that bind the localizing motifs of *Nrn1* and *Hmgb1* mRNAs. RNAs corresponding to rat *Nrn1*

nt 95–188 and *Hmgb1* nt 706–766 (NM_012963.2) were used as "target RNAs." *Nrn1* nt 1–94 and *Hmgb1* nt 2170–2230, a nonlocalizing GC-matched 3′UTR segment, were used as "control RNAs." A second control for each RAMS consisted of biotin-saturated SA beads ("biotin control") (27). SDS/PAGE showed many bound proteins under all three conditions, but target RNA binding was clearly different from control RNA and biotin control (supplemental Fig. S1*D*).

MS analyses showed many proteins bound to localizing motifs of *Nrn1* and *Hmgb1* mRNAs. Replicate RAMS assays were normalized for protein yields across the individual pull-downs for target RNAs, control RNAs, and biotin controls (supplemental Table S2*B*–S2*C*). We tested for protein enrichment in the *Nrn1* nt 95-188 and *Hmgb1* nt 706-766 pull-downs by two different analytic approaches. First, we compared relative enrichment of target *versus* control RNA using *QSpec*, which tests for differential expression in spectral count data using a generalized linear mixed effects model and hierarchical Bayes estimation (31). *QSpec* analysis showed several proteins enriched in the *Nrn1* nt 95–188 and *Hmgb1* nt 706–766 pull-downs compared with their control RNAs (Fig. 2*A*–2*B*, supplemental Table S3*A*–S3*B*). Second, we incorporated the biotin control interactions into consideration by calculating an "RNA target enrichment index" (supplemental Table S2*A*) and comparing this to spectral counts normalized for molecular weight to account for relative protein yields. Several proteins showed enriched binding to *Nrn1* nt 95–188 and *Hmgb1* nt 706–766 compared with controls (Fig. 2*C*–2*D*). Proteins with significant enrichment for *Nrn1* nt 95–188 and *Hmgb1* nt 706–766 binding were largely consistent between the two analyses, and the "high specificity interactors" for these localization motifs notably include several known RBPs (Fig. 2*A*–2*D*).

As only a few high specificity interactors overlapped between *Nrn1* nt 95–188 and *Hmgb1* nt 706–766, we expanded the data set to test for RBPs binding to *Gap43*'s 3′UTR AU rich element (ARE; nt 1211–1250, NM_017195.3) and *Actb*'s 3′UTR localization motif (nt 1206–1261, NM_031144.3) (8). The axonal localization and translational regulation of *Gap43* and *Actb* mRNAs are distinct from those of *Nrn1* and *Hmgb1* (8, 39), so we reasoned these mRNAs would provide a rigorous test for potential RBP sharing between motifs. Because known RBPs also purified with the control *Nrn1* and *Hmgb1* RNA sequences, we used a scrambled oligonucleotide as control RNA in the *Gap43* and *Actb* pull downs to determine if those RBPs represented nonspecific RNA interactions. High specificity interacting proteins were seen in RAMS for both *Gap43* and *Actb* mRNA motifs (supplemental Fig. S2*C*–S2*H* and supplemental Tables S2*D*–S2*E*, S3*C*–S3*D*). Some RBPs were shared with the *Nrn1* and *Hmgb1* mRNA localization motifs, however no high specificity interacting protein was shared by the *Nrn1, Hmgb1, Gap43,* and *Actb* mRNAs motifs (Fig. 2*F*, Table I).

Gene Ontology (GO) analyses for both summed high specificity interactors for *Nrn1, Hmgb1, Gap43,* and *Actb* motifs and for *Nrn1* nt 1–94, *Hmgb1* nt 2170–2230 and scrambled RNA showed a preponderance of nucleic acid binding terms, including RNA binding and splicing (supplemental Fig. S3). Even though these GO terms are clearly distinct from those of biotin, there were only minor differences between GO terms highlighted for axon localizing RNA motifs and control RNAs (supplemental Fig. S3). This is perhaps not a surprising finding given RNA was the bait for both purifications. Nonetheless, the GO analyses show greater enrichment for RNA interacting categories for *Nrn1* and *Hmgb1* control RNAs than for the scrambled RNA probe (supplemental Fig. S3).

Axonal hnRNPs Interact with Nrn1 and Hmgb1 mRNAs—Immunoblotting was used to validate the RNA affinity pull-down for *Nrn1* nt 95–188 and *Hmgb1* nt 706–766 high specificity interactors. Higher levels of hnRNP H1, hnRNP F, hnRNP A3, PurA, and PurB were pulled down with *Nrn1* nt 95–188 than with *Nrn1* nt 1–94, and higher levels of hnRNP K, ELAVL1, PurA, and PurB were pulled down with *Hmgb1* nt 706–766 than with *Hmgb1* nt 2170–2230. Further in accordance with RAMS data, higher levels of hnRNP K, ELAVL1, and Ncl were pulled down with *Nrn1* nt 1–94 than with *Nrn1* nt 95–188 (Fig. 2*E*). Notably, hnRNP H1 and F showed higher binding to *Hmgb1* nt 706–766 than to *Hmgb1* nt 2170–2230, and neither of these proteins were identified as *Hmgb1* nt 706–766 high specificity interactors (Fig. 2*B*, 2*E*). However, calculating enrichment indices from raw spectral counts showed enrichment indices of 0.62 ± 0.09 and 0.63 ± 0.05 for hnRNP H1 and hnRNP F, respectively (normalized enrichment indices were hnRNP H1 $= 0.42 \pm 0.12$ and hnRNP F $= 0.43 \pm 0.11$). Thus, our normalization procedure for the RAMS analyses is stringent to a degree that a few real interactors may be discarded, paying the price of a few false negatives for robustness of the final prioritized candidates. Indeed, every protein that was identified as a high specificity interactor for *Nrn1* nt 95–188 and *Hmgb1* nt 706–766 was validated by immunoblotting (Fig. 2*E*), except for hnRNP AB and Kars, for which suitably specific antibodies are not available.

The studies above show that several RBPs localize to peripheral nerve axons and some interact with the localizing motifs in *Nrn1*'s 5′UTR and *Hmgb1*'s 3′UTR at high specificity. We then asked if the endogenous *Nrn1* and *Hmgb1* mRNAs might bind to these axonal RBPs. Antibodies to hnRNP H1, F, and K proved suitable for immunoprecipitation (IP) from sciatic nerve axoplasm (Fig. 3*A*). Reverse transcription-coupled droplet digital PCR (RTddPCR) revealed that *Nrn1* and *Hmgb1* mRNAs were enriched in the hnRNP K IPs compared with control. Both mRNAs were detected in the hnRNP H1 IPs, but only *Nrn1* mRNA was significantly enriched (Fig. 3*B*–3*C*). Unfortunately, lower RNA quantities were isolated from hnRNP F IPs and no significant enrichment of *Nrn1* or

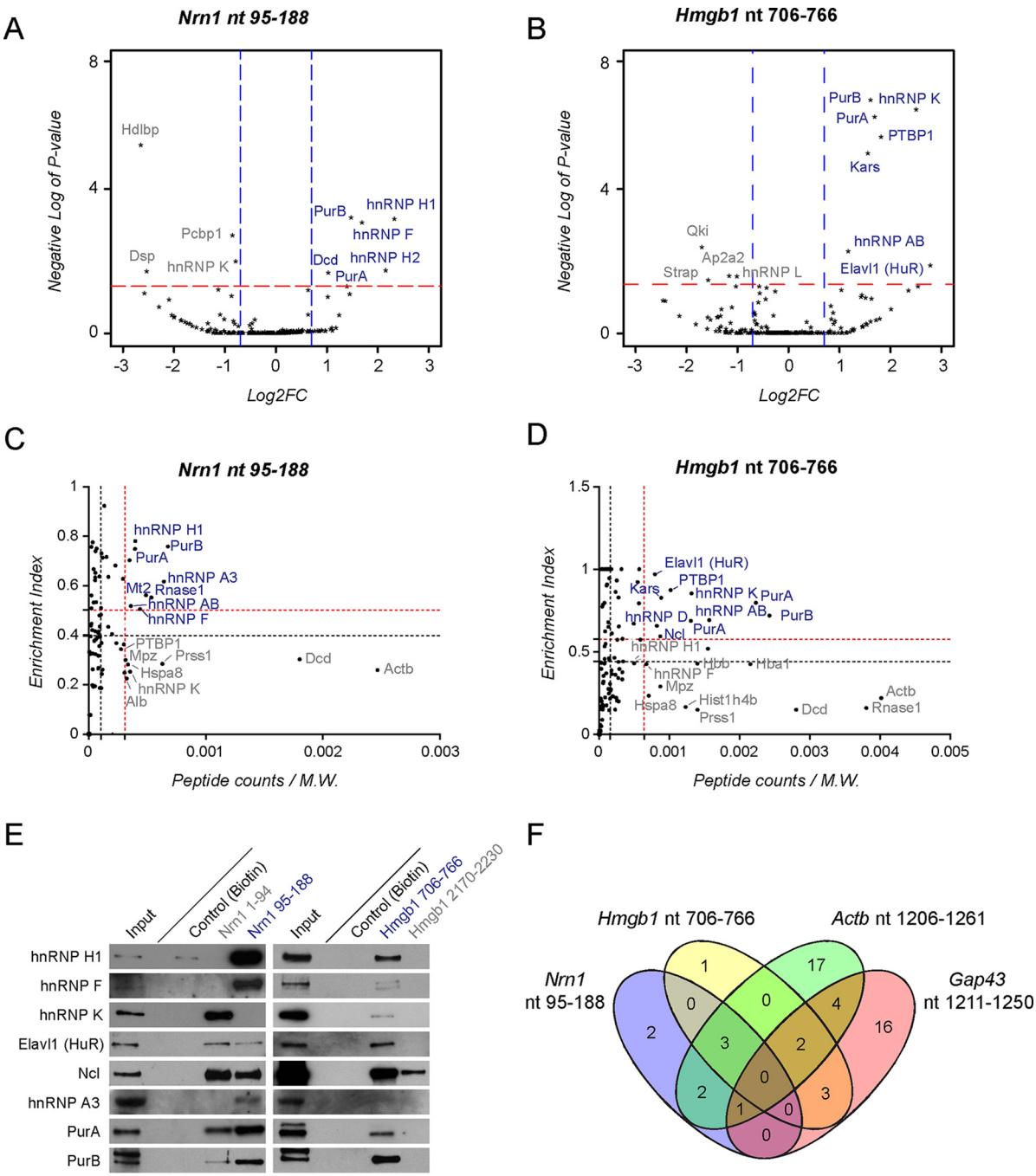

FIG. 2. **Identification of proteins interacting with axon localizing RNA motifs.** *A–B,* Volcano plots from *QSpec* analyses of RAMS data for axonal mRNA motifs *versus* control RNAs of *Nrn1* (*A*) and *Hmgb1* (*B*) are shown. Only protein hits with false-discovery rates (FDR) ≤ 0.05 over three biological replicates are included. Thresholds of 0.7 and −0.7 for log2FC (blue vertical lines) and 0.05 for *p* value (red horizontal line) are shown. Candidate proteins with enriched binding to localizing motifs are in blue font, and those with enriched binding to control RNAs are in gray font. See supplemental Tables S2 and S3 for spectral count data and analyses. *C–D,* Target RNA enrichment indices from RAMS data for *Nrn1* nt 95–188 *versus Nrn1* nt 1–95 plus biotin-saturated beads (*C*) and *Hmgb1* nt 706–766 *versus Hmgb1* nt 2,170–2,230 plus biotin-saturated beads (*D*) are shown relative to the protein spectral counts normalized to molecular weight. The black hatched lines indicate median values and red hatched lines indicate 99% confidence intervals (CI). Proteins showing high specificity interactions with target RNA are in blue font, and those showing higher interactions with control RNA and beads are in gray font. Refer to and supplemental Fig. S2*A*–S2*B* for analyses of *Nrn1* 1–94 and *Hmgb1* 2170–2230. *E,* Representative immunoblots for sciatic nerve axoplasm protein binding to biotin *Nrn1* nt 1–94 and nt 95–188 (left) or *Hmgb1* nt 706–766 and nt 2,170–2,230 (right) are shown. "Input" lane shows axoplasm isolate (5%). *F,* Venn diagram representing enriched proteins shared between *QSpec* and Enrichment Index analyses for axonal localizing motifs of *Nrn1, Hmgb1, Actb,* and *Gap43* mRNAs is shown. See also Table I and supplemental Fig. S2 and S3.

TABLE I
Summary of proteins showing high specificity interaction with axonal localizing elements of Nrn1, Hmgb1, Gap43, and Actb mRNAs

	Nrn1	*Hmgb1*	*Gap43*	*Actb*
hnRNP AB	+	+	+	
PurA	+	+		+
PurB	+	+		+
hnRNP A3	+		+	+
hnRNP D		+	+	+
hnRNP F	+			+
hnRNP H1	+			+
Elavl1 (HuR)		+	+	
Kars		+	+	
hnRNP K		+	+	
Ncl		+	+	
PTBP1		+	+	
hnRNP A2B1			+	+
KHSRP			+	+
Fubp1			+	+
LOC684558			+	+
hnRNP A1			+	+
Mt2	+			
Rnase1	+			
hnRNP U			+	
PCBP2			+	
Dhx15			+	
hnRNP L			+	
PCBP3			+	
hnRNP R			+	
Ybx1			+	
Dars			+	
Ssb			+	
Pabpc1			+	
Dis3l2			+	
Puf60			+	
PTBP2			+	
Srsf3			+	
Ybx3			+	
Hdlbp			+	
PTBP3			+	
Rtcd1				+
Fubp3				+
Ahsg				+
Paics				+
Eef2				+
hnRNP H2				+
Rpsa				+
Bub3				+
Tardbp				+
Col14a1				+
hnRNP A2B1				+
Ddx1				+
hnRNP DL				+
Rtcb				+
Tial1				+
Rab5c				+

Hmgb1 mRNAs was seen in these IPs, perhaps because of lower efficiency of the anti-hnRNP F antibody (Fig. 3*A*). This co-IP of endogenous mRNAs showed that H1 and K can bind to *Nrn1* mRNA, which is not surprising because the RAMS data indicated that hnRNP H1 interacts with *Nrn1* nt 95–188 and hnRNP K interacts with *Nrn1* nt 1–94 (Fig. 2*A*, 2*E* and supplemental Fig. S2*A*). To determine if the select interaction of hnRNP H1 and F with *Nrn1* mRNA nt 95–188 is unique to the synthetic RNAs used for RAMS, we asked if a *Flag-tagged Nrn1* mRNA would still co-IP with hnRNP H1 and K1 in a cellular context when nt 1–94 or 95–188 were deleted. For this, DRG cultures were transfected with the *Nrn1* 5′UTR truncation constructs indicated in Fig. 3*D* and processed for immunoprecipitation with control, anti-hnRNP H1 or anti-hnRNP K antibodies. Consistent with the RAMS analyses, amplifying the *Flag-tagged Nrn1* mRNAs from these IPs showed that hnRNP H1 bound significantly more *Nrn1* mRNA nt 95–188 than nt 1–94, whereas hnRNP K bound significantly more *Nrn1* mRNA nt 1–94 compared with nt 95–188 (Fig. 3*E*). These results support the RAMS findings that different hnRNP proteins associate with axonal mRNA through interaction with distinct RNA motifs.

RNA Coimmunoprecipitation Analyses of Axonal hnRNP H1, hnRNP F, and hnRNP K Segregate Axonal mRNAs Into Growth-associated Cohorts—Recent RIP approaches in 293T and HeLa cells focused on hnRNP F and H1 as coordinators of RNA splicing (40, 41). We reasoned that the axoplasm preparations would allow us to uniquely address these RBP's cytoplasmic interactors, and specifically their axonal RNA interactors. In addition to hnRNP H1, hnRNP F, and hnRNP K, we analyzed RIP data for La/SSB, an RNA chaperone protein that also localizes to sciatic nerve axons (42). For each RIP, input RNAs were sequenced for mRNA levels and RIP-seq with anti-FLAG antibody was carried out to test for IP specificity/enrichment. Top mRNAs enriched in comparisons with both controls were identified using the *Rank-Rank Hypergeometric Overlap* (RRHO) algorithm (32) (Fig. 4*A*). All detected mRNAs were ranked for enrichment *versus* input RNA-seq and anti-FLAG antibody IP RNA-seq, and these ranks were compared using RRHO to identify a core set of mRNAs with high ranking for each RBP compared with these two control data sets. We identified 3588 enriched mRNAs for hnRNP H1, 3609 for hnRNP F, for 2557 for hnRNP K, and 1010 for La/SSB (Fig. 4*B*; supplemental Table S5). Comparison of these RBP-mRNA interactomes showed highest overlap between hnRNP H1 and F (2821 mRNAs; Fig. 4*B*), which is not unexpected based on previous studies of hnRNP H1 and F interacting mRNAs (40, 41).

To exclude nonneuronal RBP-RNA interactions from the RIP data sets, we used recently available cell-specific translatome profiles of DRGs to select neuronal-enriched mRNAs from the hnRNP H1, hnRNP F, hnRNP K, and La/SSB interactomes. Rozenbaum *et al.* (2018) used RiboTag mice (43) crossed with different Cre lines specific to sensory neurons (Adv, Islt, and Runx3) or Schwann/satellite cells (DHH) to generate HA tagged-ribosomal protein L22 (L22-HA) in a cell-specific manner (33). 6230 sensory neuron-enriched mRNAs were identified from these data by RRHO using neuronal (Adv, Islt, and Runx3) *versus* Schwann/satellite cell (DHH) Cre lines. This stringent filter yielded 1048 hnRNP H1-, 1097 hnRNP F-, 646 hnRNP K-, and 260 La/SSB-interacting neuron-enriched

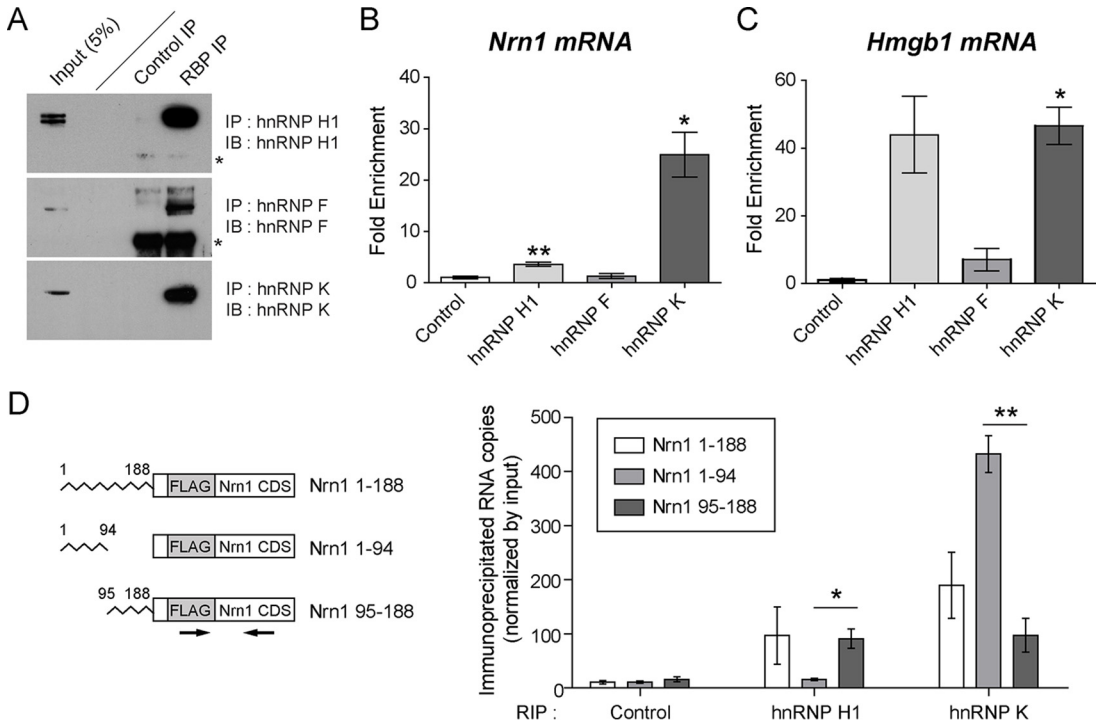

FIG. 3. **Axonal hnRNP H1 and K interact with Nrn1 and Hmgb1 mRNA.** *A,* Representative immunoblots for IP of indicated hnRNPs from sciatic nerve axoplasm is shown as indicated. FLAG antibody was used as control IP. Asterisks indicate IgG chains. *B–C,* RTddPCR for axoplasm anti-hnRNP H1, -hnRNP F, -hnRNP K and -FLAG IPs are shown. Levels of *Nrn1* and *Hmgb1* mRNAs are shown as mean fold-enrichment relative to control ± S.E. ($n = 3$; *, $p < 0.05$, **, $p < 0.01$ by one-way ANOVA with pair-wise comparison and Tukey post-hoc). *D–E,* Schematics of Nrn1 5′UTR constructs tested for co-IP with hnRNPs are shown in *D*. Arrows indicate the primer pairs used for RTddPCR amplification of *Flag-tagged Nrn1* mRNA; 3′UTR in these constructs is from the vector. Normalized RNA copy numbers for *Flag-tagged Nrn1* mRNA in the indicated IPs are shown as mean ± S.E. Copy number in input RNA was used for normalization ($n = 3$; *, $p < 0.05$, **, $p < 0.01$ by one-way ANOVA with pair-wise comparison and Tukey post-hoc).

mRNAs (Fig. 4*C*). With these data sets, overlap analyses showed that hnRNP H1 and F share 825 interacting mRNAs (62.5% of total hnRNP H1 and F-interacting mRNAs) and hnRNP H1, F, and K share 202 interacting mRNAs (12.1% of the total hnRNP H1, F, and K interacting mRNAs; Fig. 4*D*). Although enriched in the hnRNP H1, F, and K unfiltered RIP-seq data sets, *Nrn1* and *Hmgb1* mRNAs were filtered out of the neuron-enriched interactomes as these proteins derived from RRHO with DRG translatome data. This may reflect the fact that both Nrn1 and Hmgb1 are post-transcriptionally regulated after axotomy (25, 36) and the translatome data reflects translationally active mRNAs from sensory neuron soma (33).

We took three approaches to test validity of these neuron-enrichment filtered RBP-mRNA interactomes. First, FPKM values of mRNAs belonging to each RBP-interactome were extracted from the RIP-seq data set and plotted relative to fold-change in input RNA. This showed a significant enrichment for the hnRNP H1-, F-, and K-specific mRNAs as well as those mRNAs shared between H1 and F (supplemental Fig. S4). Second, RTddPCR for 35 randomly selected hnRNP H1-, F- and K-interacting mRNAs were directly tested for mRNA levels precipitating with RBPs from sciatic nerve axoplasm. mRNA copies for each RIP from RT-ddPCR analyses showed a significant linear correlation with FPKM values from the RIP-seq data (supplemental Fig. S5). The different y-intercepts for these analyses are because of different input levels for the RNA-seq and RTddPCR - the RNA-seq requires equivalent RNA mass, whereas the RTddPCR was performed based on equivalent fractions of the IPs. The weak correlation of La/SSB is likely because of the relatively low abundance of these mRNAs precipitated by La/SSB compared with other RBPs. Third, we performed *de novo* motif discovery on the neuron-enriched hnRNP H1, F, and K interactomes. The top 3 predicted hnRNP H1 and F motifs contain quite similar A/G-rich stretches, whereas motifs predicted for hnRNP K appeared distinct (Fig. 4*E*). A/G-rich motifs were also identified as direct binding motifs for hnRNP H1 in HEK 293T and HeLa cells (40, 41). Binding to *Hmgb1* mRNA was only identified HEK 293T cells, and that was an intronic RNA interaction rather than to the mRNA (44); *Nrn1* mRNA was not found in either cell line possibly because of low Nrn1 expression (40, 41).

GO term analysis showed several enriched terms and pathways shared between the hnRNP H1-, F-, and K-interacting mRNAs, with several related to axon growth mechanisms

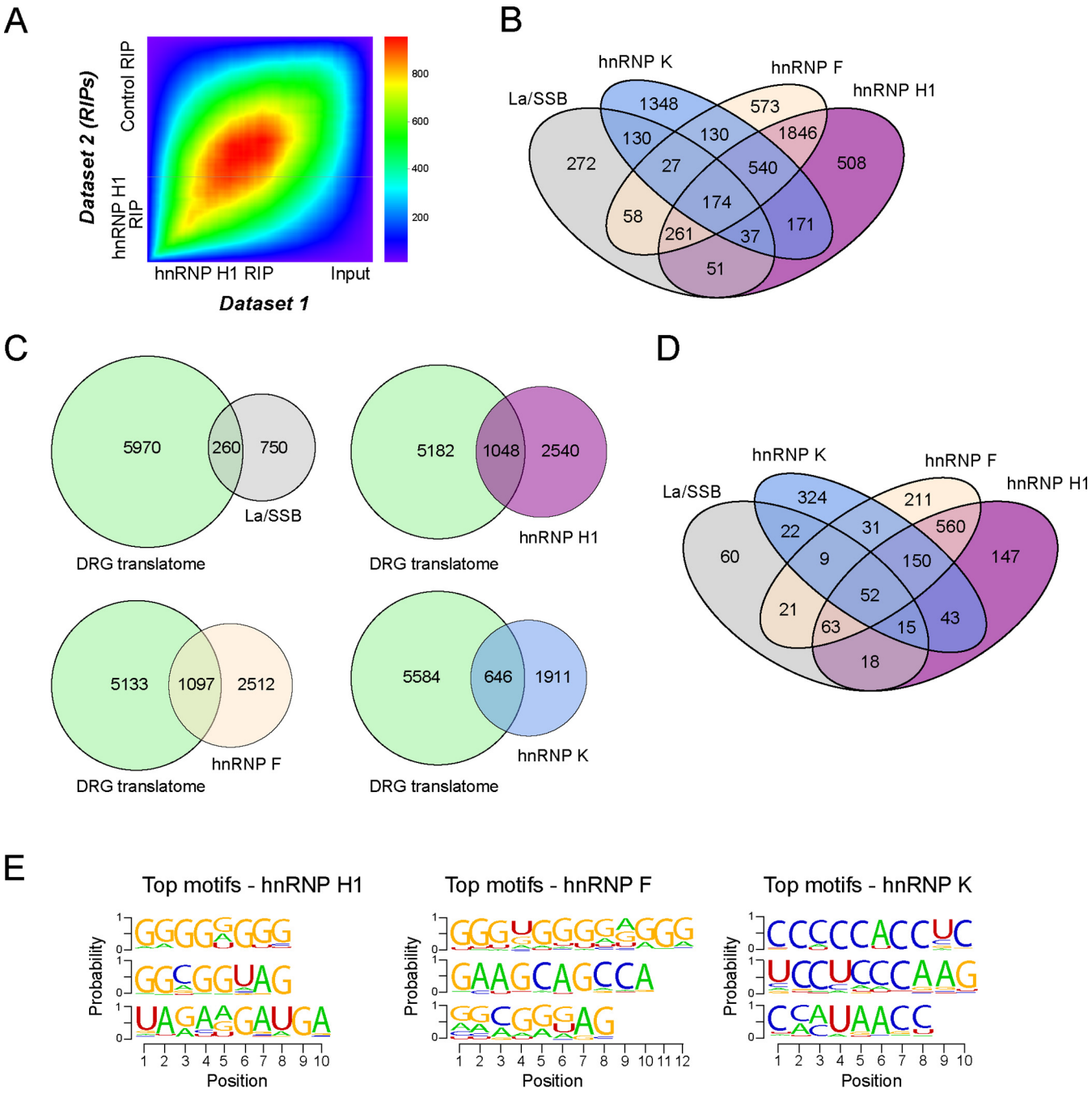

FIG. 4. **Axonal *hnRNP H1,* F and K associate with overlapping but distinct sets of mRNAs.** *A,* Representative plot for of RRHO analysis that was used to identify RBP enriched mRNAs from RNA-seq data is shown for hnRNP H1. hnRNP H1 RIP compared with input (data set 1) *versus* hnRNP H1 RIP compared with FLAG RIP (data set 2) generates a list of mRNAs showing enriched binding to hnRNP H1. Heat maps show signed log-transformed *t* test *p* values. See supplemental Table S4 for FKPM values. *B,* Venn diagram comparing La/SSB-, hnRNP H1-, hnRNP F- and hnRNP K-enriched mRNAs from RRHO of RIP-seq data is shown. See supplemental Table S5 for identified mRNAs. *C,* Overlap between neuron-enriched translatome data and La/SSB-, hnRNP H1-, hnRNP F- and hnRNP K-enriched mRNAs from *A–B* are shown as Venn diagrams. Note that this substantially decreased the complexity of the RIP-seq data. See supplemental Table S6 for identified mRNAs. *D,* Overlap between neuron-enriched interactomes of axonal hnRNP H1, hnRNP F, hnRNP K, and La/SSB are shown. *E,* Predicted highest priority RNA motifs for binding by hnRNP H1, F and K from HOMER algorithm motif discovery applied to the neuron-enriched interactomes are shown as indicated.

(supplemental Fig. S6*A*–S6*C*). In contrast, these terms did not show as enriched in the GO terms for La/SSB interactome or mRNAs identified in the axoplasm used for the IPs (*i.e.* input; supplemental Fig. S6*D*–S6*E*). Furthermore, pathway analyses of the interactomes showed that "axon guidance" was more enriched in the hnRNP interactomes than the La/SSB inter-

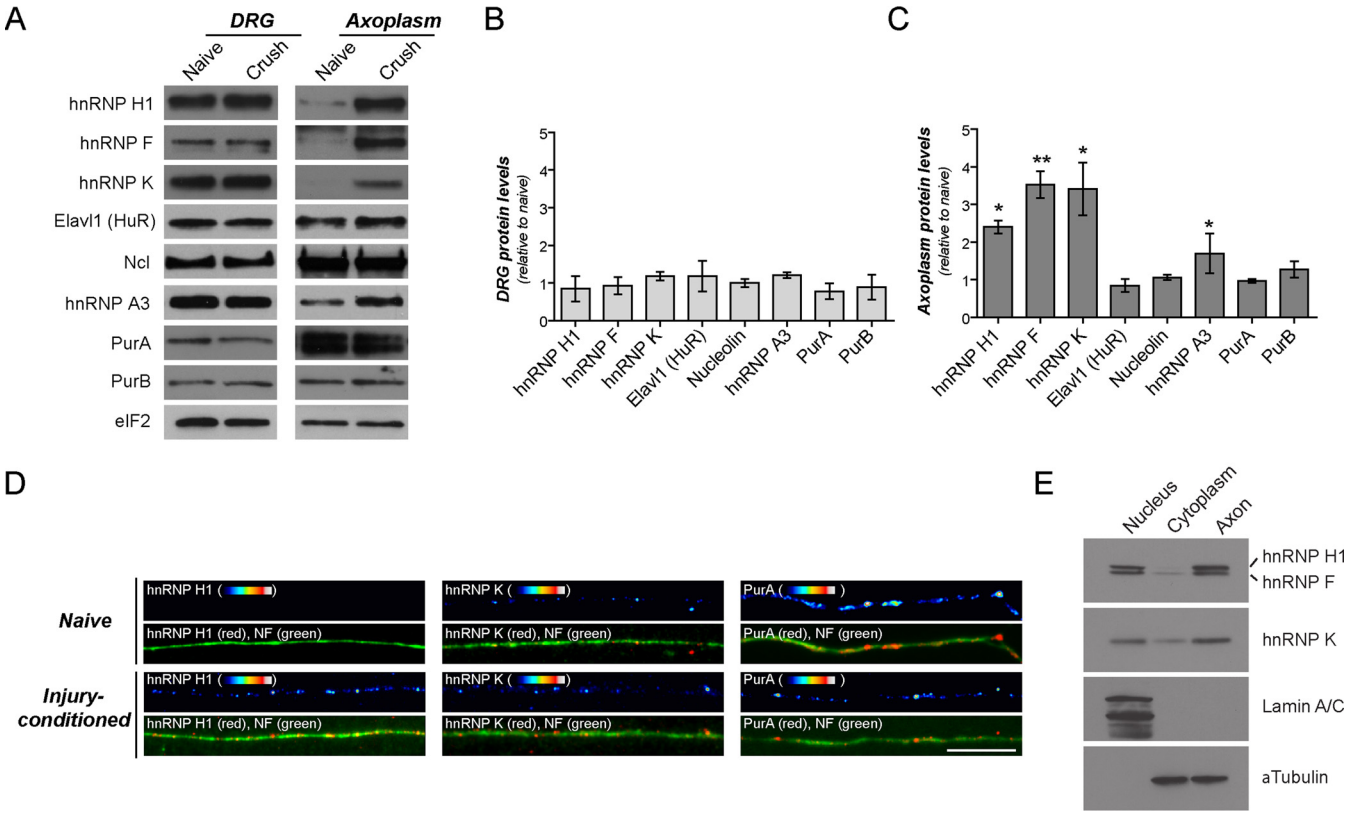

FIG. 5. **Axonal levels of hnRNP H1, F and K increase during regeneration.** *A–C,* Representative immunoblots (*A*) of sciatic nerve axoplasm (left) and L4–5 DRGs (right) from uninjured (naïve) and 7-day post-injury (crush) animals along with quantifications (*B–C*) are shown. For quantitation, data are plotted as mean fold-change relative to naïve ± S.D. ($n = 3$; *, $p < 0.05$, **, $p < 0.01$ by Student's *t* test). *D,* Representative immunofluorescence images for distal axons of dissociated DRGs cultured from naïve (upper) and 7-day injury-conditioned (lower) DRGs are shown. Columns show images matched for exposure, gain, and post-processing (Scale bar = 20 μm). See also supplemental Fig. S7. *E,* Representative immunoblot for subcellular fractions from DRG cultures. Equal amounts of proteins from nucleus, cytoplasm and axonal fractions were used to determine the relative levels of hnRNP H1, F and K. Immunoblotting for Lamin A/C and α-Tubulin shows successful fractionation of cytoplasm and nuclear proteins.

actome (supplemental Fig. S6*F*). Taken together, these data validate the RBP-mRNA interactomes developed from RRHO neuron-enrichment filtered hnRNP RIP analyses and emphasize the utility of this approach to selectively uncover RNA-protein interactions in peripheral axons.

Axonal hnRNP H1, F, and K Levels Increase with Axotomy—The GO analyses and IPA above suggest that axon growth-regulating RNA regulons are defined by hnRNP interactions. To test this possibility, we first asked if axonal levels of these proteins change during nerve regeneration. For this, we used immunoblotting to compare the relative levels of *Nrn1* nt 95–188 or *Hmgb1* nt 706–766 high specificity interacting proteins in sciatic nerve axoplasm after crush injury. Levels of hnRNP H1, F, and K were significantly increased in injured compared with naïve nerve (Fig. 5*A*, 5*C*). L4–5 DRG lysates did not show any detectable change in hnRNP H1, F, and K protein levels after nerve injury (Fig. 5*A*, 5*B*). There was also no change in levels of the mRNA encoding these proteins in injured L4–5 DRGs (data not shown), suggesting that the increased hnRNP levels in the regenerating axoplasm occur through post-translational mechanisms.

Because the studies above used extruded axoplasm, we asked if these RBPs could be visualized in distal axons. After an exhaustive trial of antibodies, fixation, and immunolabeling approaches, we identified a few RBP antibodies suitable for immunofluorescence. hnRNP H1, hnRNP K, and PurA were visualized in axons of cultured DRG neurons, and axonal signals for hnRNP H1 and K were more prominent in injury-conditioned neurons (Fig. 5*D*). The axonal RBP signals were punctate, like what has been reported for mRNAs in axons. Interestingly, the signals for hnRNP H1 and K appeared predominantly nuclear in Schwann cells, whereas the soma of the DRG neurons showed more prominent cytoplasmic signals (supplemental Fig. S7). By immunoblotting with lysates isolated from axonal, cytoplasmic and nuclear fractions of dissociated DRG cultures, levels of hnRNP H1, F and K proteins were significantly higher in nuclear compared with cytoplasm fractions (Fig. 5*E*). However, axonal isolates showed that axonal fractions contained levels of hnRNP H1, F and K proteins comparable to the nuclear fractions (Fig. 5*E*). Considering that glial cells are also included in the nuclear and cytoplasm fractions analyzed in these cultures, these data

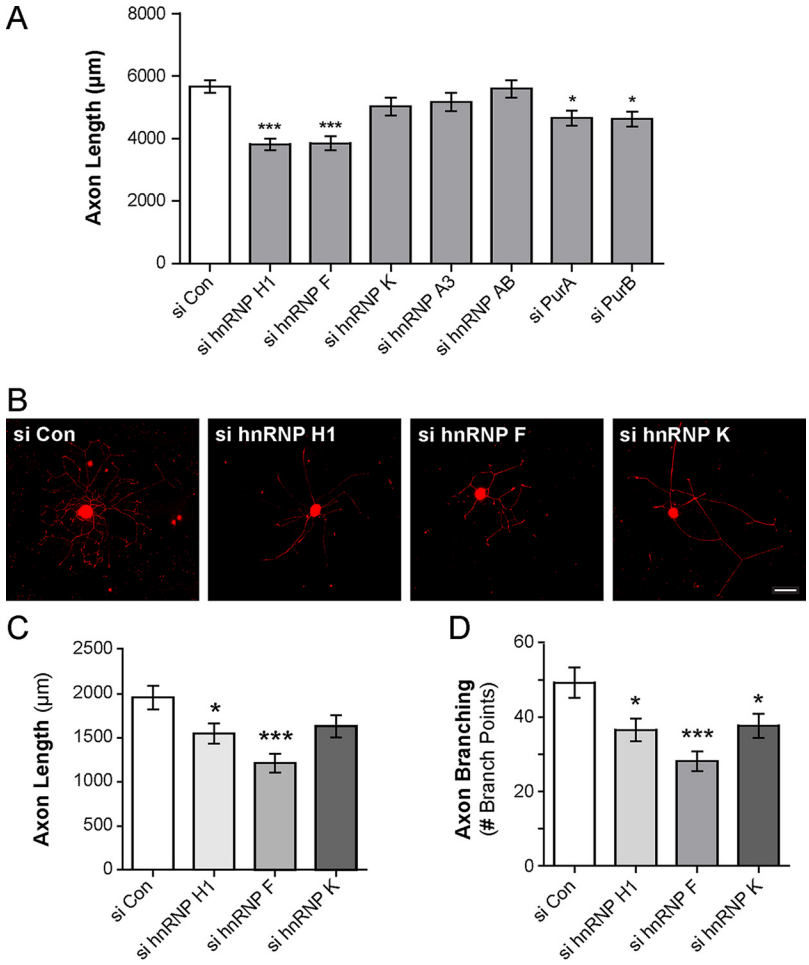

FIG. 6. **Depletion of hnRNP H1 and F alters axon outgrowth.** *A,* Total axon length from 3 DIV DRG culture after single transfection with indicated siRNAs is shown as mean fold-change ± S.E. relative to control siRNA (siCon; N ≥ 150 neurons in three independent cultures; ***, $p < 0.005$, *, $p < 0.05$ by one-way ANOVA with pair-wise comparison and Tukey post-hoc). *B–D,* Dissociated DRG neurons were sequentially transfected with siRNAs as indicated at DIV 0 and 4, and then replated on laminin-coated coverslips on DIV 6. Representative images of individual neurons stained for NF at 20 h after replating are shown in B (Scale bar = 100 µm). *C* and *D* show total axon length and branching graphed as mean ± S.E. (N ≥ 150 neurons in three independent cultures; *, $p \leq 0.05$, ***, $p < 0.005$ by one-way ANOVA with pair-wise comparison and Tukey post-hoc). See also supplemental Fig. S8.

emphasize that these hnRNPs show robust localization into the axonal compartment.

hnRNP H1 and F Function to Support Axon Growth—Axonally synthesized Nrn1 and Hmgb1 proteins support axonal outgrowth from DRG neurons (25, 36). Thus, we asked if depletion of the high specificity RBP interactors for *Nrn1* and *Hmgb1* mRNAs might affect axon growth. Axon outgrowth from cultured DRG neurons was significantly decreased at 3 days *in vitro* (DIV) after treatment with hnRNP H1 and hnRNP F siRNAs. hnRNP K, A3, and AB siRNAs had no significant effect on axon growth, whereas PurA and PurB siRNAs caused a modest, but statistically significant decrease in axon length (Fig. 6*A*). Although each of the target mRNAs was robustly depleted by the siRNAs (supplemental Fig. S8*A*), there was only modest reduction of hnRNP H1 and F proteins (immunoreactivity in soma relative to control: hnRNP H1 = 0.79 ± 0.04, $p = 0.016$ and hnRNP F = 0.81 ± 0.02; $p = 0.002$; data not shown). High stability of these RBPs might explain the mismatch between hnRNP H1 and F protein and mRNA levels with the siRNA transfections. To address this possibility, we used sequential siRNA transfections at DIV 0 and 4 that brought greater reduction of the proteins (supplemental Fig. S8*B*–S8*D*). There was more reduction in axon length for hnRNP H1- and F-depleted DRGs as well as decreased axon branching in hnRNP H1-, F-, and K-depleted DRGs (supplemental Fig. S8*B*–S8*D*). Together, these data point to axon growth functions for hnRNP H1, F, and K in adult sensory neurons, which is consistent with functional predictions derived from RAMS and subsequent RIP-seq analyses.

Combined Depletion of hnRNP H1, H2, and F Decreases Axonal mRNA Translation—Despite that axon growth was affected by siRNA-mediated decreases in hnRNP H1, F, and K, axonal levels of *Nrn1* and *Hmgb1* showed no change with these knockdowns (data not shown). hnRNP H1 is known to form a heterodimer with hnRNP F (45). hnRNP H2 has not been studied extensively but it is highly homologous to hnRNP H1, with greater 95% primary sequence identity. Thus, hnRNP H1, H2, and F could share functions, which is consistent with the overlapping mRNA interactomes of hnRNP H1 and F shown above. This also raises the possibility for compensation by hnRNP H1, H2, or F upon deletion of a single depletions of hnRNP H1, H2, or F. To test this possibility, we performed double and triple knockdown hnRNP H1 + H2 and hnRNP H1 + H2 + F (supplemental Fig. S9*A*). Single knockdown of hnRNP H2 had no significant effect on axon length or branching (Fig. 7*A*–7*B*). Combined knockdown of hnRNP

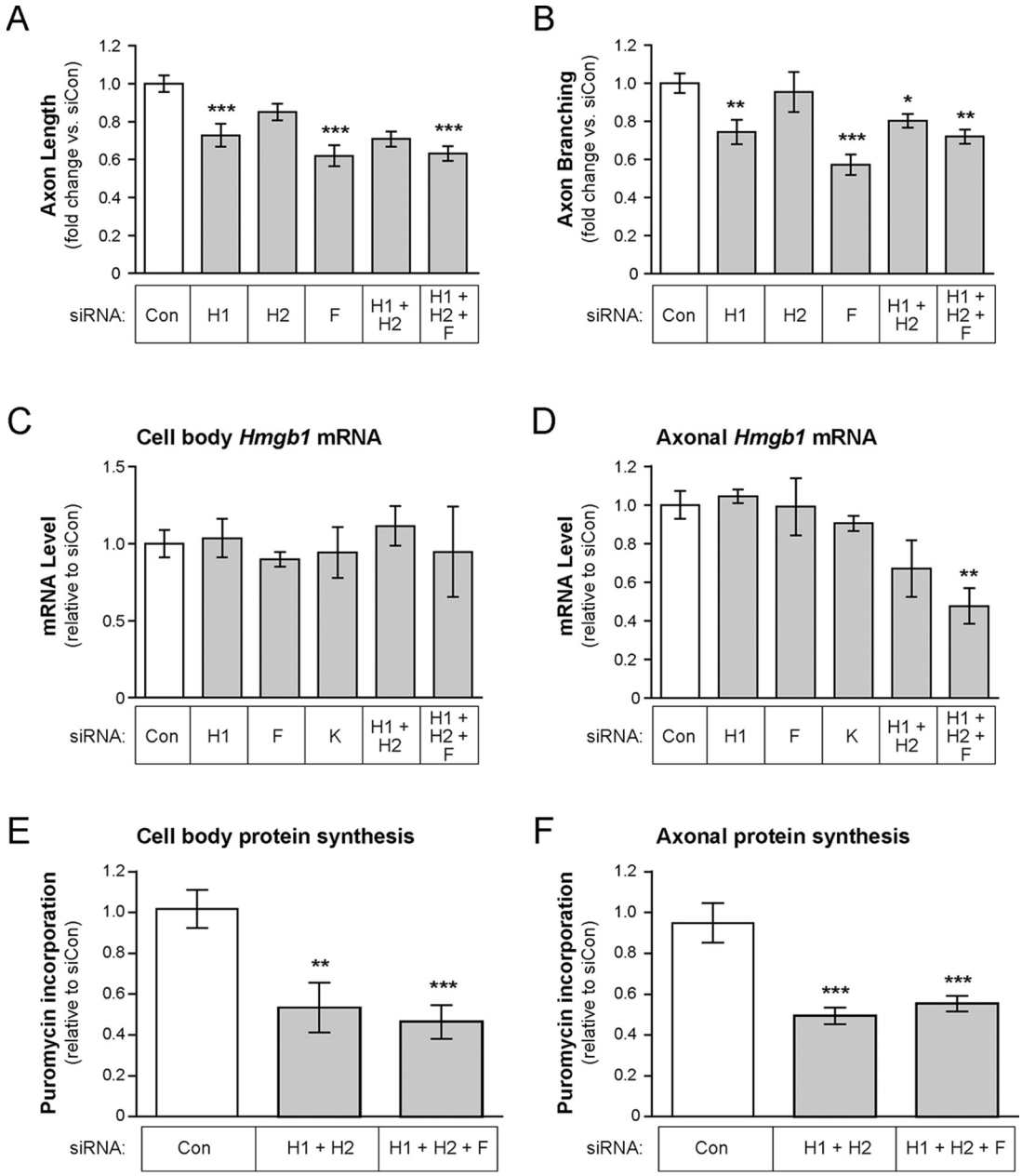

FIG. 7. **Depletion of hnRNP H1, H2 and F together decreases axonal mRNA and translation.** *A–B,* DRG neurons were transfected with siRNAs against indicated RBPs and then replated on laminin with axon length and branching analyzed 24 h later. Total axon length (*A*) and branching (*B*; branch point number/per neuron) are shown as mean fold change *versus* siCon ± S.E. (N ≥ 200 neurons in three independent cultures; *, $p \leq 0.05$, **, $p \leq 0.01$, ***, $p < 0.005$ by one-way ANOVA with pair-wise comparison and Tukey post-hoc). See supplemental Fig. S9*A* for siRNA efficiency. *C–D,* RTddPCR for *Hmgb1* mRNA in cell body (*C*) and axonal (*D*) preparations from DRG cultures transfected with indicated siRNAs is shown as mean fold change relative to siCon ± S.E. ($n = 3$; **, $p < 0.01$ by one-way ANOVA with pair-wise comparison and Tukey post-hoc). *Nrn1* mRNA did not show any significant changes (see supplemental Fig. S9*B*). *E–F,* Puromycin incorporation in cell body (*E*) and axons (*F*) of cultured DRG neurons transfected with indicated siRNAs was used to test for nascent protein synthesis. Values are shown as mean fold change relative to siCon ± S.E. (N ≥ 20 cells or 50 axons in three independent cultures; **, $p \leq 0.01$, ***, $p < 0.005$ by one-way ANOVA with pair-wise comparison and Tukey post-hoc).

H1 + H2 and hnRNP H1 + H2 + F did not result in significant further reduction of axon length or branching compared with the single knockdowns of hnRNP H1 or F (Fig. 7*A*–7*B*). Despite no additive or synergistic effects with double and triple knockdowns, there was a significant decrease in axonal *Hmgb1* mRNA with hnRNP H1 + H2 + F siRNA transfections (Fig. 7*C*–7*D*). Axonal *Nrn1* mRNA showed some decreases in both cell body and axons with these depletions but none reached statistical significance (supplemental Fig. S9*B*–S9*C*). Puromycinylation assays also showed decreased translation

in axons and cell bodies after knockdown of hnRNP H1 + H2 and hnRNP H1 + H2 + F (Fig. 7*E*–7*F*). These data suggest overlapping functions of hnRNP H1, H2, and F for post-transcriptional regulation of gene expression in sensory neurons.

DISCUSSION

Axons of sensory, cortical, hippocampal, retinal ganglion, and motor neurons have been shown to contain complex mRNA populations by RNA-seq analyses of isolated axons (18, 19, 46–50). Despite identifying thousands of axonal mRNAs, exceptionally few RBPs have been found to date in axons. We used an unbiased proteomics approach to identify axonal RBPs that interact with the localizing motifs of *Nrn1*, *Hmgb1*, *Actb,* and *Gap43* mRNAs. These four axonal mRNAs are regulated by injury-induced axonal localization, injury-induced intra-axonal translation, neurotrophin-induced transport/translation, and injury-induced transcription-coupled axonal localization, respectively (6, 8, 22, 25, 36). We observed a surprising diversity of RBPs showing high specificity binding to these mRNA localization motifs. Axonal localization was not previously known for most of the identified RBPs. No high specificity interacting proteins were shared between all four mRNA localization motifs, suggesting the existence of multiple mRNA-protein complexes defined by composition of RBPs interacting with these mRNA motifs. RIP-seq analyses for the RBPs further distinguished hnRNPs F, H1, and K as high specificity interactors for *Nrn1* and *Hmgb1* mRNAs. Axonal mRNAs encoding proteins linked to axon growth are enriched in the mRNA interactomes for hnRNP H1, F, and K compared with mRNAs enriched in the La/SSB interactome and those in the input axoplasm RNA-seq. Taken together, our data provide a unique and novel resource for axonal RBP-mRNA interactomes that will be a critical step in understanding *in vivo* mRNA dynamics in PNS axons.

The RBPs tested here are predominantly nuclear-localized in Schwann cells, but in neurons are at high levels in the axons. This suggests additional cytoplasmic and axonal functions for these RBPs in post-mitotic neurons, perhaps because of the much greater expanses of cytoplasm that neurons must grow and sustain with their long axonal processes. Multifunctionality has been documented for several RBPs, including axonal ZBP1, FMRP, nucleolin, and HuD that contribute to transport and stability or transport and translation of neuronal mRNAs (6, 51–54). Both the RIP-seq data and depletion studies point to functions in axonal growth for hnRNP H1, F, and K. It will be of high interest to determine the molecular mechanisms for growth promotion by these hnRNPs and distinguish nuclear and somatic *versus* axonal functions for these proteins. A few hnRNPs have been shown to impact neuronal differentiation and axon development (55–57). However, no studies have considered subcellular functions for these hnRNPs. Our data show that these hnRNPs can interact with mRNAs at centimeters distance from the neuronal soma. hnRNP K has been shown to regulate nuclear export and translation of *Nfm* and *Gap43* mRNAs whose protein products contribute to axon growth (58). Our identification of hnRNP K as a high specificity interacting protein for *Gap43* points to intra-axonal functions for hnRNP K in regulating *Gap43*. Because many of the RBPs we identified are known to have nuclear functions, it is appealing to speculate that interactions between hnRNPs and axonally targeted mRNAs may initiate in the nucleus and persist into the axons.

Increased attention to post-transcriptional regulation in neurons has fueled efforts to identify components of their RNA transport granules. Several groups have profiled the protein content of RNPs from brain extracts using affinity purification or differential sedimentation techniques (59–62). There is substantial overlap between proteins in these RNP isolates and the RBPs identified herein. Overlapping proteins include numerous hnRNPs, splicing factors/RNA helicases, translation-related proteins, RNA degradation-related proteins, and other RBPs known to be present in neurons (59–62). Compared with these previous studies, the axoplasm used here provides a unique view of a subcellular compartment that is biologically relevant for RNA transport and localized protein synthesis. The axoplasm preparation method used here has previously been shown to be highly enriched in axonal proteins compared with non-neuronal proteins (63), indicating that the RAMS approach used here has uncovered RNA-interacting proteins from axons. The RBP-mRNA interactomes established here provide a cohort of bound axonal mRNAs that can be tested in the future for direct *versus* indirect RBP interactions. Nonetheless, there are limitations to the RAMS approach used here. First, both HuD and ZBP1 are known to bind to the localization motifs of *Gap43* and *Actb*, but these proteins were not identified here (supplemental Table S2). The axoplasm preparation is enriched in axonal protein constituents but detergents are not used for isolation (24). Thus, RBPs that interact with cytoskeleton, such as HuD and ZBP1, would be missed in the RAMS. Second, the stringency we used for normalization of biological replicates unavoidably causes false negatives, with some relevant bound proteins failing significance criteria in the *QSpec* and enrichment index analyses. hnRNP F and H1 binding to *Hmgb1* nt 706–766 in the validation studies above are evidence of this. However, these stringent criteria increase confidence in the high specificity interactors identified by RAMS.

Axotomy is known to change neuronal gene expression programs, and this is in part by altering axonal transport of cargo proteins (64, 65). The increased levels that we found for hnRNP F, H1, and K in regenerating axons most likely occurs through post-transcriptional mechanisms (Fig. 6*C*–6*D*). Either increased transport into axons, local translation or increased stability within axons could account for these changes. Interestingly, the increased levels of axonal hnRNP F and H1 are in line with the increase in axonal *Nrn1* transport after PNS nerve injury, and the increase in axonal hnRNP K corresponds to the

increase in *Hmgb1* translation seen in regenerating axons (25, 36). Post-translational modifications have been shown to alter activity and/or subcellular localization of a few RBPs (6, 42, 66, 67). Thus, it will be of high interest to determine how more hnRNP F, H1 and K proteins localize into regenerating axons, particularly because knockdown of these proteins affects axon growth and combined knockdown of hnRNP H1, H2, and F decreased protein synthesis in axons.

In summary, we have identified RBPs that interact with localizing motifs of *Nrn1*, *Hmgb1, Actb,* and *Gap43* mRNAs in regenerating sciatic nerve, substantially increasing the number of known axonal RBPs. The majority of the RBPs identified here were found to interact with only one or two of the four axonal mRNA localization motifs tested. MS analyses of proteins interacting with the RBPs Staufen and Barentsz in embryonic rat brain indicate at least two distinct dendritic RNP populations (60), and multiple dendritic RNPs have been defined by DEAD box protein content (68). Thus, the RBPs identified in the RAMS analyses here most likely constitute unique protein combinations for cohorts of axonally localizing mRNAs. This is supported by our RNA profiling of axonal hnRNP-bound mRNAs, which segregates axonal mRNAs into functional groups highly suggestive of subcellular RNA regulons.

Acknowledgments—The authors thank Jill Turner, Sofia Lizarraga, Fabienne Poulain, and Deanna S. Smith for constructive comments and guidance. MS experiments were performed at the Biomedical Mass Spectrometry Resource at UCSF supported by funding from the Howard Hughes Medical Institute (to ALB). JLT is the Endowed SmartState Chair in Childhood Neurotherapeutics at the Univ. South Carolina. MF is the incumbent of the Chaya Professorial Chair in Molecular Neuroscience at the Weizmann Institute of Science.

DATA AVAILABILITY

Data for protein identifications based on single peptides are available as individual annotated spectra at http://prospector.ucsf.edu/prospector/mshome.htm (see supplemental Table S7 for accession numbers). Raw and processed RNA co-immunoprecipitation sequencing data were deposited within the Gene Expression Omnibus (GEO) repository (www.ncbi.nlm.nih.gov/geo, accession number: GSE103444). The raw MS proteomics data have been deposited in the Mass Spectrometry Interactive Virtual Environment (*MassIVE*) with the data set identifier MSV000081910.

* This work was supported by grants from NIH (R01-NS041596 to JLT, 8P41-GM103481 to ALB, 1P20GM109091-01 to MS, R03-DA043428-01A1 to MS), the Dr. Miriam and Sheldon G. Adelson Medical Research Foundation (to ALB, GC, MF and JLT) and ASPIRE grant from the Office of the Vice President for Research at the University of South Carolina (to SJL). The content is solely the responsibility of the authors and does not necessarily represent the official views of the National Institutes of Health or other funding sources.

S This article contains supplemental Figures and Tables. The authors have no financial conflicts of interest for the work reported here.

§§ To whom correspondence should be addressed: Department of Biological Sciences, University of South Carolina, 715 Sumter Street, CLS 401, Columbia, SC 29208. Tel.: 803-777-9215; Fax: 803-777-4002; E-mail: twiss@mailbox.sc.edu.

Author contributions: S.J.L., A.N.K., and J.L.T. designed research; S.J.L., J.A.O.-P., R.K., P.K.S., A.N.K., M.R., S.C., S.M.-R., and R.J.T. performed research; S.J.L., J.A.O.-P., R.K., P.K.S., D.O., S.C., H.J., M.S., M.F., G.C., A.L.B., and J.L.T. analyzed data; S.J.L., R.K., and J.L.T. wrote the paper; J.A.O.-P., R.K., M.R., D.O., M.S., M.F., G.C., and A.L.B. contributed new reagents/analytic tools.

REFERENCES

1. Sahoo, P. K., Smith, D. S., Perrone-Bizzozero, N., and Twiss, J. L. (2018) Axonal mRNA transport and translation at a glance. *J. Cell Sci.* 131 pii: jcs196808
2. Rangaraju, V., Tom Dieck, S., and Schuman, E. M. (2017) Local translation in neuronal compartments: how local is local? *EMBO Reports* **18,** 693–711
3. Terenzio, M., Schiavo, G., and Fainzilber, M. (2017) Compartmentalized Signaling in Neurons: From Cell Biol. to Neuroscience. *Neuron* **96,** 667–679
4. Hornberg, H., and Holt, C. (2013) RNA-binding proteins and translational regulation in axons and growth cones. *Front. Neurosci.* **7,** 81
5. Gomes, C., Merianda, T. T., Lee, S. J., Yoo, S., and Twiss, J. L. (2014) Molecular determinants of the axonal mRNA transcriptome. *Dev. Neurobiol.* **74,** 218–232
6. Huttelmaier, S., Zenklusen, D., Lederer, M., Dictenberg, J., Lorenz, M., Meng, X., Bassell, G. J., Condeelis, J., and Singer, R. H. (2005) Spatial regulation of beta-actin translation by Src-dependent phosphorylation of ZBP1. *Nature* **438,** 512–515
7. Kim, H. H., Lee, S. J., Gardiner, A. S., Perrone-Bizzozero, N. I., and Yoo, S. (2015) Different motif requirements for the localization zipcode element of beta-actin mRNA binding by HuD and ZBP1. *Nucleic Acids Res.* **43,** 7432–7446
8. Yoo, S., Kim, H. H., Kim, P., Donnelly, C. J., Kalinski, A. L., Vuppalanchi, D., Park, M., Lee, S. J., Merianda, T. T., Perrone-Bizzozero, N. I., and Twiss, J. L. (2013) A HuD-ZBP1 ribonucleoprotein complex localizes GAP-43 mRNA into axons through its 3′ untranslated region AU-rich regulatory element. *J. Neurochem.* **126,** 792–804
9. Cosker, K. E., Fenstermacher, S. J., Pazyra-Murphy, M. F., Elliott, H. L., and Segal, R. A. (2016) The RNA-binding protein SFPQ orchestrates an RNA regulon to promote axon viability. *Nat. Neurosci.* **19,** 690–696
10. Zhang, P., Abdelmohsen, K., Liu, Y., Tominaga-Yamanaka, K., Yoon, J. H., Ioannis, G., Martindale, J. L., Zhang, Y., Becker, K. G., Yang, I. H., Gorospe, M., and Mattson, M. P. (2015) Novel RNA- and FMRP-binding protein TRF2-S regulates axonal mRNA transport and presynaptic plasticity. *Nat. Commun.* **6,** 8888
11. Donnelly, C. J., Willis, D. E., Xu, M., Tep, C., Jiang, C., Yoo, S., Schanen, N. C., Kirn-Safran, C. B., van Minnen, J., English, A., Yoon, S. O., Bassell, G. J., and Twiss, J. L. (2011) Limited availability of ZBP1 restricts axonal mRNA localization and nerve regeneration capacity. *EMBO J.* **30,** 4665–4677
12. Antar, L. N., Li, C., Zhang, H., Carroll, R. C., and Bassell, G. J. (2006) Local functions for FMRP in axon growth cone motility and activity-dependent regulation of filopodia and spine synapses. *Mol. Cell Neurosci.* **32,** 37–48
13. Williams, K. R., McAninch, D. S., Stefanovic, S., Xing, L., Allen, M., Li, W., Feng, Y., Mihailescu, M. R., and Bassell, G. J. (2016) hnRNP-Q1 represses nascent axon growth in cortical neurons by inhibiting Gap-43 mRNA translation. *Mol. Biol. Cell* **27,** 518–534
14. Glinka, M., Herrmann, T., Funk, N., Havlicek, S., Rossoll, W., Winkler, C., and Sendtner, M. (2010) The heterogeneous nuclear ribonucleoprotein-R is necessary for axonal beta-actin mRNA translocation in spinal motor neurons. *Hum. Mol. Genet.* **19,** 1951–1966
15. Fallini, C., Bassell, G. J., and Rossoll, W. (2012) The ALS disease protein TDP-43 is actively transported in motor neuron axons and regulates axon outgrowth. *Hum. Mol. Genet.* **21,** 3703–3718
16. Hornberg, H., Wollerton-van Horck, F., Maurus, D., Zwart, M., Svoboda, H., Harris, W. A., and Holt, C. E. (2013) RNA-binding protein Hermes/RBPMS inversely affects synapse density and axon arbor formation in retinal ganglion cells in vivo. *J. Neurosci.* **33,** 10384–10395

17. Perry, R. B., Rishal, I., Doron-Mandel, E., Kalinski, A. L., Medzihradszky, K. F., Terenzio, M., Alber, S., Koley, S., Lin, A., Rozenbaum, M., Yudin, D., Sahoo, P. K., Gomes, C., Shinder, V., Geraisy, W., Huebner, E. A., Woolf, C. J., Yaron, A., Burlingame, A. L., Twiss, J. L., and Fainzilber, M. (2016) Nucleolin-mediated RNA localization regulates neuron growth and cycling cell size. *Cell Reports* **16,** 1664–1676
18. Minis, A., Dahary, D., Manor, O., Leshkowitz, D., Pilpel, Y., and Yaron, A. (2014) Subcellular transcriptomics-dissection of the mRNA composition in the axonal compartment of sensory neurons. *Dev. Neurobiol.* **74,** 365–381
19. Saal, L., Briese, M., Kneitz, S., Glinka, M., and Sendtner, M. (2014) Subcellular transcriptome alterations in a cell culture model of spinal muscular atrophy point to widespread defects in axonal growth and presynaptic differentiation. *RNA* **20,** 1789–1802
20. Keene, J. D. (2007) RNA regulons: coordination of post-transcriptional events. *Nat. Rev. Genet* **8,** 533–543
21. Twiss, J. L., Smith, D. S., Chang, B., and Shooter, E. M. (2000) Translational control of ribosomal protein L4 mRNA is required for rapid neurite regeneration. *Neurobiol. Dis.* **7,** 416–428
22. Willis, D. E., van Niekerk, E. A., Sasaki, Y., Mesngon, M., Merianda, T. T., Williams, G. G., Kendall, M., Smith, D. S., Bassell, G. J., and Twiss, J. L. (2007) Extracellular stimuli specifically regulate localized levels of individual neuronal mRNAs. *J. Cell Biol.* **178,** 965–980
23. Rishal, I., Kam, N., Perry, R. B., Shinder, V., Fisher, E. M., Schiavo, G., and Fainzilber, M. (2012) A motor-driven mechanism for cell-length sensing. *Cell Reports* **1,** 608–616
24. Hanz, S., Perlson, E., Willis, D., Zheng, J. Q., Massarwa, R., Huerta, J. J., Koltzenburg, M., Kohler, M., van Minnen, -J., Twiss, J. L., and Fainzilber, M. (2003) Axoplasmic importins enable retrograde injury signaling in lesioned nerve. *Neuron* **40,** 1095–1104
25. Merianda, T. T., Gomes, C., Yoo, S., Vuppalanchi, D., and Twiss, J. L. (2013) Axonal localization of neuritin/CPG15 mRNA in neuronal populations through distinct 5′ and 3′ UTR elements. *J. Neurosci.* **33,** 13735–13742
26. Vuppalanchi, D., Coleman, J., Yoo, S., Merianda, T. T., Yadhati, A. G., Hossain, J., Blesch, A., Willis, D. E., and Twiss, J. L. (2010) Conserved 3′-untranslated region sequences direct subcellular localization of chaperone protein mRNAs in neurons. *J. Biol. Chem.* **285,** 18025–18038
27. Doron-Mandel, E., Alber, S., Oses, J. A., Medzihradszky, K. F., Burlingame, A. L., Fainzilber, M., Twiss, J. L., and Lee, S. J. (2016) Isolation and analyses of axonal ribonucleoprotein complexes. *Methods Cell Biol.* **131,** 467–486
28. Rosenfeld, J., Capdevielle, J., Guillemot, J. C., and Ferrara, P. (1992) In-gel digestion of proteins for internal sequence analysis after one- or two-dimensional gel electrophoresis. *Anal. Biochem.* **203,** 173–179
29. Guan, S., Price, J. C., Prusiner, S. B., Ghaemmaghami, S., and Burlingame, A. L. (2011) A data processing pipeline for mammalian proteome dynamics studies using stable isotope metabolic labeling. *Mol. Cell. Proteomics* **10,** M111.010728
30. Clauser, K. R., Baker, P., and Burlingame, A. L. (1999) Role of accurate mass measurement (+/- 10 ppm) in protein identification strategies employing MS or MS/MS and database searching. *Anal. Chem.* **71,** 2871–2882
31. Choi, H., Fermin, D., and Nesvizhskii, A. I. (2008) Significance analysis of spectral count data in label-free shotgun proteomics. *Mol. Cell. Proteomics* **7,** 2373–2385
32. Plaisier, S. B., Taschereau, R., Wong, J. A., and Graeber, T. G. (2010) Rank-rank hypergeometric overlap: identification of statistically significant overlap between gene-expression signatures. *Nucleic Acids Res.* **38,** e169
33. Rozenbaum, M., Rajman, M., Rishal, I., Koppel, I., Koley, S., Medzihradszky, K. F., Oses-Prieto, J. A., Kawaguchi, R., Amieux, P. S., Burlingame, A. L., Coppola, G., and Fainzilber, M. (2018) Translatome Regulation in Neuronal Injury and Axon Regrowth. *eNeuro* **5,** e0276-0217.2018
34. Eden, E., Navon, R., Steinfeld, I., Lipson, D., and Yakhini, Z. (2009) GOrilla: a tool for discovery and visualization of enriched GO terms in ranked gene lists. *BMC Bioinformatics* **10,** 48
35. Yu, G., Wang, L. G., Han, Y., and He, Q. Y. (2012) clusterProfiler: an R package for comparing biological themes among gene clusters. *OMICS* **16,** 284–287
36. Merianda, T. T., Coleman, J., Kim, H. H., Kumar Sahoo, P., Gomes, C., Brito-Vargas, P., Rauvala, H., Blesch, A., Yoo, S., and Twiss, J. L. (2015) Axonal amphoterin mRNA is regulated by translational control and enhances axon outgrowth. *J. Neurosci.* **35,** 5693–5706
37. Rishal, I., Golani, O., Rajman, M., Costa, B., Ben-Yaakov, K., Schoenmann, Z., Yaron, A., Basri, R., Fainzilber, M., and Galun, M. (2013) WIS-NeuroMath enables versatile high throughput analyses of neuronal processes. *Dev. Neurobiol.* **73,** 247–256
38. Li, X., Quon, G., Lipshitz, H. D., and Morris, Q. (2010) Predicting in vivo binding sites of RNA-binding proteins using mRNA secondary structure. *RNA* **16,** 1096–1107
39. Zhang, H. L., Eom, T., Oleynikov, Y., Shenoy, S. M., Liebelt, D. A., Dictenberg, J. B., Singer, R. H., and Bassell, G. J. (2001) Neurotrophin-induced transport of a beta-actin mRNP complex increases beta-actin levels and stimulates growth cone motility. *Neuron* **31,** 261–275
40. Huelga, S. C., Vu, A. Q., Arnold, J. D., Liang, T. Y., Liu, P. P., Yan, B. Y., Donohue, J. P., Shiue, L., Hoon, S., Brenner, S., Ares, M., Jr, and Yeo, G. W. (2012) Integrative genome-wide analysis reveals cooperative regulation of alternative splicing by hnRNP proteins. *Cell Reports* **1,** 167–178
41. Uren, P. J., Bahrami-Samani, E., de Araujo, P. R., Vogel, C., Qiao, M., Burns, S. C., Smith, A. D., and Penalva, L. O. (2016) High-throughput analyses of hnRNP H1 dissects its multi-functional aspect. *RNA Biol.* **13,** 400–411
42. van Niekerk, E. A., Willis, D. E., Chang, J. H., Reumann, K., Heise, T., and Twiss, J. L. (2007) Sumoylation in axons triggers retrograde transport of the RNA-binding protein La. *Proc. Natl. Acad. Sci. U.S.A.* **104,** 12913–12918
43. Sanz, E., Yang, L., Su, T., Morris, D. R., McKnight, G. S., and Amieux, P. S. (2009) Cell-type-specific isolation of ribosome-associated mRNA from complex tissues. *Proc. Natl. Acad. Sci. U.S.A.* **106,** 13939–13944
44. Huelga, S. C., Vu, A. Q., Arnold, J. D., Liang, T. Y., Liu, P. P., Yan, B. Y., Donohue, J. P., Shiue, L., Hoon, S., Brenner, S., Ares, M., Jr, and Yeo, G. W. (2012) Integrative genome-wide analysis reveals cooperative regulation of alternative splicing by hnRNP proteins. *Cell Reports* **1,** 167–178
45. Matunis, M. J., Xing, J., and Dreyfuss, G. (1994) The hnRNP F protein: unique primary structure, nucleic acid-binding properties, and subcellular localization. *Nucleic Acids Res.* **22,** 1059–1067
46. Briese, M., Saal, L., Appenzeller, S., Moradi, M., Baluapuri, A., and Sendtner, M. (2016) Whole transcriptome profiling reveals the RNA content of motor axons. *Nucleic Acids Res.* **44,** e33
47. Shigeoka, T., Jung, H., Jung, J., Turner-Bridger, B., Ohk, J., Lin, J. Q., Amieux, P. S., and Holt, C. E. (2016) Dynamic axonal translation in developing and mature visual circuits. *Cell* **166,** 181–192
48. Zivraj, K. H., Tung, Y. C., Piper, M., Gumy, L., Fawcett, J. W., Yeo, G. S., and Holt, C. E. (2010) Subcellular Profiling Reveals Distinct and Developmentally Regulated Repertoire of Growth Cone mRNAs. *J. Neurosci.* **30,** 15464–15478
49. Taylor, A. M., Berchtold, N. C., Perreau, V. M., Tu, C. H., Li Jeon, N., and Cotman, C. W. (2009) Axonal mRNA in uninjured and regenerating cortical mammalian axons. *J. Neurosci.* **29,** 4697–4707
50. Baleriola, J., Walker, C. A., Jean, Y. Y., Crary, J. F., Troy, C. M., Nagy, P. L., and Hengst, U. (2014) Axonally synthesized ATF4 transmits a neurodegenerative signal across brain regions. *Cell* **158,** 1159–1172
51. Li, C., Bassell, G. J., and Sasaki, Y. (2009) Fragile X mental retardation protein is involved in protein synthesis-dependent collapse of growth cones induced by semaphorin-3A. *Front. Neural. Circuits* **3,** 11
52. Smith, C. L., Afroz, R., Bassell, G. J., Furneaux, H. M., Perrone-Bizzozero, N. I., and Burry, R. W. (2004) GAP-43 mRNA in growth cones is associated with HuD and ribosomes. *J. Neurobiol.* **61,** 222–235
53. Perry, R. B., Rishal, I., Doron-Mandel, E., Kalinski, A. L., Medzihradszky, K. F., Terenzio, M., Alber, S., Koley, S., Lin, A., Rozenbaum, M., Yudin, D., Sahoo, P. K., Gomes, C., Shinder, V., Geraisy, W., Huebner, E. A., Woolf, C. J., Yaron, A., Burlingame, A. L., Twiss, J. L., and Fainzilber, M. (2016) Nucleolin-mediated RNA localization regulates neuron growth and cycling cell size. *Cell Reports* **16,** 1664–1676
54. Terenzio, M., Koley, S., Samra, N., Rishal, I., Zhao, Q., Sahoo, P. K., Urisman, A., Marvaldi, L., Oses-Prieto, J. A., Forester, C., Gomes, C., Kalinski, A. L., Di Pizio, A., Doron-Mandel, E., Perry, R. B., Koppel, I., Twiss, J. L., Burlingame, A. L., and Fainzilber, M. (2018) Locally translated mTOR controls axonal local translation in nerve injury. *Science* **359,** 1416–1421

55. Grammatikakis, I., Zhang, P., Panda, A. C., Kim, J., Maudsley, S., Abdelmohsen, K., Yang, X., Martindale, J. L., Motino, O., Hutchison, E. R., Mattson, M. P., and Gorospe, M. (2016) Alternative splicing of neuronal differentiation factor TRF2 regulated by HNRNPH1/H2. *Cell Reports* **15,** 926–934
56. Liu, Y., Gervasi, C., and Szaro, B. G. (2008) A crucial role for hnRNP K in axon development in Xenopus laevis. *Development* **135,** 3125–3135
57. Hutchins, E. J., and Szaro, B. G. (2013) c-Jun N-terminal kinase phosphorylation of heterogeneous nuclear ribonucleoprotein K regulates vertebrate axon outgrowth via a posttranscriptional mechanism. *J. Neurosci.* **33,** 14666–14680
58. Liu, Y., Yu, H., Deaton, S. K., and Szaro, B. G. (2012) Heterogeneous nuclear ribonucleoprotein K, an RNA-binding protein, is required for optic axon regeneration in Xenopus laevis. *J. Neurosci.* **32,** 3563–3574
59. Elvira, G., Wasiak, S., Blandford, V., Tong, X. K., Serrano, A., Fan, X., del Rayo Sanchez-Carbente, M., Servant, F., Bell, A. W., Boismenu, D., Lacaille, J. C., McPherson, P. S., DesGroseillers, L., and Sossin, W. S. (2006) Characterization of an RNA granule from developing brain. *Mol. Cell. Proteomics* **5,** 635–651
60. Fritzsche, R., Karra, D., Bennett, K. L., Ang, F. Y., Heraud-Farlow, J. E., Tolino, M., Doyle, M., Bauer, K. E., Thomas, S., Planyavsky, M., Arn, E., Bakosova, A., Jungwirth, K., Hormann, A., Palfi, Z., Sandholzer, J., Schwarz, M., Macchi, P., Colinge, J., Superti-Furga, G., and Kiebler, M. A. (2013) Interactome of two diverse RNA granules links mRNA localization to translational repression in neurons. *Cell Reports* **5,** 1749–1762
61. Kanai, Y., Dohmae, N., and Hirokawa, N. (2004) Kinesin transports RNA: isolation and characterization of an RNA-transporting granule. *Neuron* **43,** 513–525
62. Krichevsky, A. M., and Kosik, K. S. (2001) Neuronal RNA granules: a link between RNA localization and stimulation-dependent translation. *Neuron* **32,** 683–696
63. Rishal, I., Michaelevski, I., Rozenbaum, M., Shinder, V., Medzihradszky, K. F., Burlingame, A. L., and Fainzilber, M. (2010) Axoplasm isolation from peripheral nerve. *Dev. Neurobiol.* **70,** 126–133
64. Perry, R. B., and Fainzilber, M. (2014) Local translation in neuronal processes–in vivo tests of a "heretical hypothesis". *Dev. Neurobiol.* **74,** 210–217
65. Saito, A., and Cavalli, V. (2016) Signaling Over Distances. *Mol. Cell. Proteomics* **15,** 382–393
66. Narayanan, U., Nalavadi, V., Nakamoto, M., Pallas, D. C., Ceman, S., Bassell, G. J., and Warren, S. T. (2007) FMRP phosphorylation reveals an immediate-early signaling pathway triggered by group I mGluR and mediated by PP2A. *J. Neurosci.* **27,** 14349–14357
67. Narayanan, U., Nalavadi, V., Nakamoto, M., Thomas, G., Ceman, S., Bassell, G. J., and Warren, S. T. (2008) S6K1 phosphorylates and regulates fragile X mental retardation protein (FMRP) with the neuronal protein synthesis-dependent mammalian target of rapamycin (mTOR) signaling cascade. *J. Biol. Chem.* **283,** 18478–18482
68. Miller, L. C., Blandford, V., McAdam, R., Sanchez-Carbente, M. R., Badeaux, F., DesGroseillers, L., and Sossin, W. S. (2009) Combinations of DEAD box proteins distinguish distinct types of RNA: protein complexes in neurons. *Mol. Cell Neurosci.* **40,** 485–495